IEEE Access
Multidisciplinary | Rapid Review | Open Access Journal

Received May 16, 2021, accepted May 26, 2021, date of publication June 4, 2021, date of current version June 15, 2021.

Digital Object Identifier 10.1109/ACCESS.2021.3086423

Optimal Adaptive Super-Twisting Sliding-Mode Control Using Online Actor-Critic Neural Networks for Permanent-Magnet Synchronous Motor Drives

FAYEZ F. M. EL-SOUSY, (Member, IEEE), AND FARHAN A. F. ALENIZI, (Member, IEEE)
Electrical Engineering Department, College of Engineering, Prince Sattam bin Abdulaziz University, Al-Kharj 16278, Saudi Arabia

Corresponding author: Fayez F. M. El-Sousy (f.elsousy@psau.edu.sa)

This work was supported by the Deanship of Scientific Research, Prince Sattam bin Abdulaziz University, Saudi Arabia, under Grant 9362/01/2018.

ABSTRACT In this paper, a novel optimal adaptive-gains super-twisting sliding-mode control (OAGSTSMC) using actor-critic approach is proposed for a high-speed permanent-magnet synchronous motor (PMSM) drive system. First, the super-twisting sliding-mode controller (STSMC) is adopted for reducing the chattering phenomenon and stabilizing the PMSM drive system. However, the control performance may be destroyed due external disturbances and parameter variations of the drive system. In addition, the conservative selection of the STSMC gains may affect the control performance. Therefore, for enhancing the standard super-twisting approach performance via avoiding the constraints on knowing the disturbances as well as uncertainties upper bounds, and to achieve the drive system robustness, the direct heuristic dynamic programming (HDP) is utilized for optimal tuning of STSMC gains. Consequently, an online actor-critic algorithm with HDP is designed for facilitating the online solution of the Hamilton-Jacobi-Bellman (HJB) equation via a critic neural network while pursuing an optimal control via an actor neural network at the same time. Furthermore, based on Lyapunov approach, the stability of the closed-loop control system is assured. A real-time implementation is performed for verifying the proposed OAGSTSMC efficacy. The experimental results endorse that the proposed OAGSTSMC control approach achieves the PMSM superior dynamic performance regardless of unknown uncertainties as well as exterior disturbances.

INDEX TERMS Actor-critic neural network, adaptive control, adaptive dynamic programming, high-speed PMSM, Hamilton-Jacobi-Bellman, Lyapunov stability, optimal control, super-twisting sliding-mode control.

I. INTRODUCTION

Recently, numerous processing methods of micro-electromechanical systems (MEMS) have been industrialized for minimizing the power dissipation, the weight, and the size of the micromotors. For particular industrial applications, micromotors are deliberated as promising nominees to accomplish high-performance operation. The micro permanent-magnet synchronous motors (micro PMSMs) have high robustness, high efficiency, better reliability, along with high speed operation in comparison with further micromotors [2], [3]. Moreover, micro PMSMs are promising candidates for numerous practical applications e.g. power driving devices in MEMS, surgical devices, medical diagnostic, security equipment, along with micro autonomic robots [4].

Numerous control approaches have been investigated for micromotors [1], [5]–[12], [14]–[20]. A comparative analysis of inverter topologies has been carried out and a 6-phase 5-level inverter has been designed as well as verified experimentally at a high frequency of 2 MHz [5]. Encoderless speed control approaches have been presented [6]–[12]. For micro PMSMs encoderless control, the rotor position angle is estimated in the control approaches [6], [7]. In [8]–[10], an observer for estimating the rotor position angle of the micro PMSM along with robust H_∞ controller have been presented. The investigation of encoderless control of slotless PMSM without current control loops is developed in [11] and the three-phase back emfs are estimated via first-order delay

The associate editor coordinating the review of this manuscript and approving it for publication was Choon Ki Ahn.

filter to construct the three-phase voltages are accomplished in [12]. An intelligent Petri-fuzzy neural network (PFNN) controller as well as a robust identifier have been introduced in [13] for micro PMSM system. In [14], an adaptive inverse control approach including an adaptive controller has been introduced. In [15], an optimal design of encoderless-based speed controller has been introduced. Furthermore, a motion controller containing an optimal position controller along with a tuning parameter feed-forward controller has been introduced for micro PMSM system [16]. A sliding-mode observer (SMO) has been presented as a robust encoderless control approach for high-speed micro PMSM in [17]. A novel nonlinear controller has been designed using an adaptive backstepping controller with recurrent radial basis function neural network (RRBFNN) uncertainty estimator along with robust control for fulfilling the PMSM robust performance [18], [19]. In [20], an adaptive backstepping robust optimal control technique for accomplishing high-dynamic response of micro PMSM drive has been proposed. The optimality and robustness of the control performance are achieved by adding a nonlinear optimal controller to the adaptive backstepping controller. The optimal control input can be approximated via employing the critic neural network for online Hamilton-Jacobi-Bellman (HJB) solution via the adaptive dynamic programming (ADP).

Because the PMSM is a nonlinear system, the linearization nearby one operating point cannot be employed for designing the controller. Thus, for resolving this problem, nonlinear control approaches are successfully employed. Sliding-mode controller (SMC) can be generally utilized because of its ease of realization along with robustness alongside both uncertainties along with external disturbances. The SMC possess a variable control system structure with less sensitivity alongside parameter variations along with exterior disturbances [21]–[31]. In [28], traditional SMC state-of-the-art over soft computing was introduced. The SMC suffers from the chattering problem that is appeared as noise in the output variables due to the switching at high frequency of the control input. The mixing between the sliding-mode techniques along with fuzzy-logic-based approach [24] has developed as an alternative technique for dealing with control systems characterized through nonlinearity along with uncertainties. Though, the SMC technique is a robust approach and can control the nonlinear systems, it undergoes from the chattering phenomenon. An indirect adaptive fuzzy SMC was presented in [25] to deal with the chattering problem for the nonlinear systems. For evading the SMC chattering problem, various techniques have been utilized such as intelligent along with adaptive approaches in [21], [24] along with high-order SMC techniques in [32]–[51]. In [36], STSMC as well as high order sliding-mode observer have been utilized to control along with estimate the altitude velocity of unmanned aircraft system. The STSMC has been introduced in [39] for coping with the chattering phenomenon that can occur in traditional SMC. The output of the feedback control via STSMC was investigated for perturbed double-integrator system. In [40], [41] a Lyapunov-based super-twisting adaptive SMC has been introduced. The dynamical adapted control gains have been employed for guaranteeing the establishment of a 2^{nd} order sliding mode [42]. In [43], a super-twisting algorithm via 2^{nd} order sliding-mode observer (2-SMO) is developed to avoid the chattering problem in traditional SMO for PMSM drive. In [44], a variable-gain super-twisting algorithm based Lyapunov theory is proposed to alleviate the chattering phenomenon for linear time invariant systems. In [45], a second-order sliding-mode control is proposed to enhance the dynamic performances for LC-coupling hybrid active power filter. In [46], a composite supertwisting sliding mode control via backstepping is designed to improve the dynamic behavior of the nonlinear magnetic levitation systems. In [47], an adaptive super-twisting sliding mode control via nonlinear fractional-order PID scheme and extended state observer for controlling the speed of the PMSM drive is developed to accomplish high dynamic performance as a result of external disturbance. In [48], an adaptive sliding mode control strategy is built based on the high-order sliding mode control to effectively decrease the chattering of the system and decrease the errors of the observer and repress the mismatch of the system model. In [49], an adaptive super-twisting sliding-mode observer is built considering the nonlinear behavior of the VSI for sensorless control of the PMSM drive. In [50], a higher-order super-twisting sliding-mode observer (SMO) is proposed for dropping chattering and singularity happening in traditional SMO. An adaptive super-twisting SMO in conjunction with moving average filter via phase-locked loop is designed to estimate the speed of PMSM accurately. In [51], a super-twisting sliding-mode observer (SMO) with the model reference adaptive system (MRAS) for sensorless control of linear induction motor drives is proposed. In addition, a super-twisting SMO via Popov's hyperstability theory is adopted for stator current observer.

Based on the above discussion, it is clear that super-twisting sliding mode-based controllers possess an intrinsic robustness alongside parameter disparities along with exterior disturbances. However, the control of high-speed PMSM drive systems using the STSMC technique carries novel challenges that have not been yet straight introduced in the aforementioned researches or have not been elucidated in an adequate manner. Specifically, both the robustness as well as optimal parameter tuning characteristics in the super-twisting control approaches should be taking into account in the STSMC design for PMSM in order to follow a target trajectory with the best accuracy in presence of parameter uncertainties along with exterior disturbances. Although in the literature, the control approaches for the high-speed motors can guarantee the stability, but the controller optimal design did not considered. This optimal control approach should ensure the stability of the closed-loop system as well as reduce the controller cost. Accordingly, the optimal controller design is generally important in practical applications.

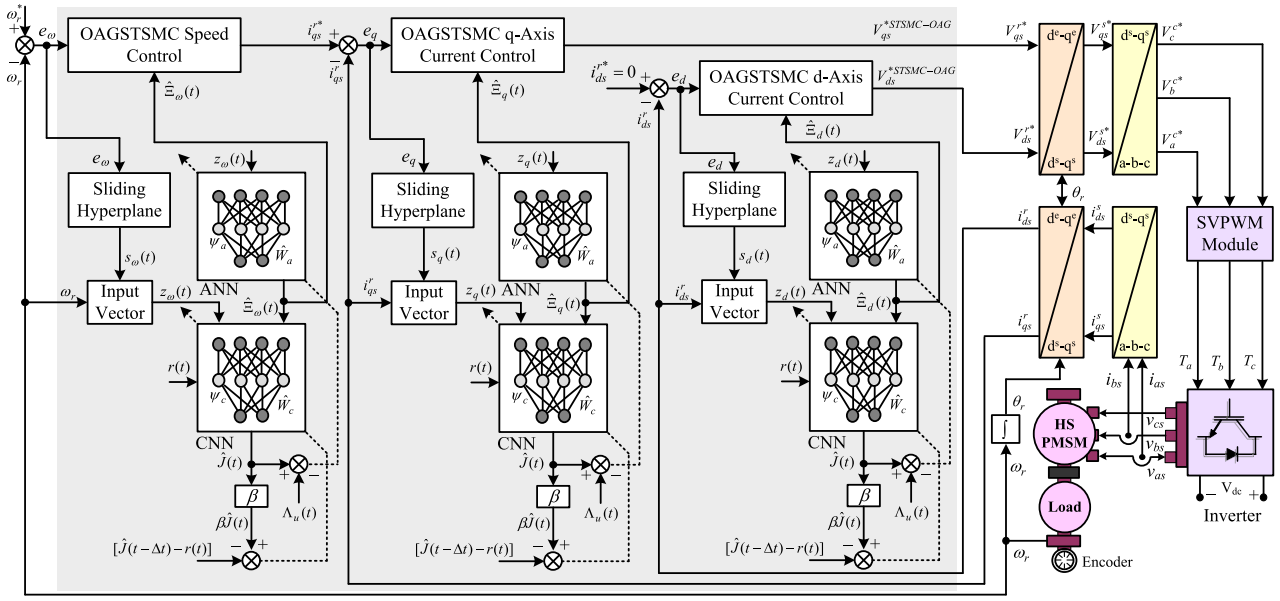

FIGURE 1. The proposed OAGSTSMC for PMSM drive system.

The nonlinear optimal control obstacle always entails solving the HJB equation that comprises solving nonlinear partial differential equations [52], [53]. Nevertheless, adaptive dynamic programming (ADP) has been utilized in solving the problems of the optimal control, it undergoes from the curse of dimensionality, which was primarily because of the backward-in-time approach. For avoiding this struggle, based on function approximation, ADP has been presented by Werbos in [54] as an approach for coping with the problems of the optimal control forward-in-time. Therefore, ADP is considered an effective approach which can solve the optimal control problems. The problem of the optimal control can be converted to the solution of HJB equation, which is a nonlinear partial differential equation for time varying systems [55]–[57]. ADP technique has been utilized for solving the problems of the optimal tracking control as discussed in [58]–[63]. Furthermore for nonlinear systems in [64]–[71], online approaches for solving the continuous HJB equation have been presented using neural networks. ADP approaches can be classified into heuristic dynamic programming (HDP), dual heuristic dynamic programming (DHP), globalized DHP (GDHP). For these approaches, there exists an action dependent (AD) versions such as AD heuristic dynamic programming (ADHDP) and AD dual heuristic dynamic programming (ADDHP) [54], [55], [72]–[76]. The HDP is one of the adaptive critic design approaches that can provide a method of computing both the optimal control along with the value function via approximations [54]. Through this approach, the curse of dimensionality can be addressed. For efficiently computing the optimal solutions, the DHP as well as the GDHP as an adaptive critic structures has been proposed [55].

The aim of this paper is designing an OAGSTSMC approach using actor-critic neural network for the PMSM drive. Fig. 1 depicts the drive system structure of the proposed OAGSTSMC. For practical applications, the compounded disorders along with precise lumped parameter uncertainties are difficult to be known before the PMSM control operation. Therefore, a novel nonlinear control approach is considered based on the super-twisting sliding-mode control with optimal adaptive-gains with actor-critic neural networks along with adaptive dynamic programming for fulfilling the target optimal performance. Via employing Lyapunov stability theorem, the OAGSTSMC technique is constructed for accurately controlling the PMSM rotor angular speed. First, an improved STSMC is adopted as the robust concept for reducing the chattering phenomenon and achieving the trajectory tracking of the PMSM drive system. Following this, actor-critic neural networks via direct HDP (ACNN-HDP) approach is employed for optimal tuning of the STSMC gains. For a robust response of the super-twisting control approach in coping with uncertainties, complex disturbances, along with optimal performance of the HDP-based control systems, an OAGSTSMC is proposed that accomplishes entirely the stated properties. The proposed control design validation is endorsed through the simulation and verified experimentally at the parameter uncertainties. The major achievements of this paper include:

1) Developing a novel optimal adaptive-gains super-twisting sliding-mode control via actor-critic based HDP control configuration.
2) Considering the robustness and optimal parameter tuning characteristics in the design of the STSMC to achieve the high-dynamic performance in presence of parameter uncertainties and exterior disturbances.
3) Improving the performance in terms of best accuracy of trajectory tracking and disturbance rejection capabilities in comparison with the conventional STSMC is achieved.

4) Designing online optimal tuning algorithms for STSMC parameter based on HDP approach that reduces the control effort and the chattering level to achieve an optimal performance.
5) Applying Lyapunov-based adaptive strategy to the STSMC to reduce the control efforts and improve the control performance.

This paper is structured as: Section II introduces the mathematical model of the PMSM with disparity in parameters and exterior disorders. In Section III, the standard form of the STSMC algorithm and the stability analysis are addressed. Section IV includes the design procedures of the OAGSTSMC scheme with actor-critic neural networks and HDP. Furthermore, Section IV introduces the adaptive training methods along with the stability study of the proposed OAGSTSMC technique. The dSPACE DS1102 is employed for implementing the proposed control approaches. The PMSM drive has been studied for investigating the dynamic response throughout the extrinsic load disturbances. Section V presents the validation results for endorsing the OAGSTSMC effectiveness for the PMSM. Section VI concludes the paper and summarizes the contributions of the paper.

II. MATHEMATICAL MODELING AND PROBLEM FORMULATION

A. PMSM DYNAMIC MATHEMATICAL MODEL

The field oriented control (FOC) technique is widely employed for the PMSM control. The FOC aims to achieve a high-torque aptitude for the PMSM. The PMSM analytical modeling in the rotating reference frame is expressed by (1) & (2) [18]–[20]:

$$V_{qs}^{r} = R_s i_{qs}^{r} + L_{ss}\frac{d}{dt} i_{qs}^{r} + \omega_r L_{ss} i_{ds}^{r} + \omega_r \lambda_m' \tag{1}$$

$$V_{ds}^{r} = R_s i_{ds}^{r} + L_{ss}\frac{d}{dt} i_{ds}^{r} - \omega_r L_{ss} i_{qs}^{r} \tag{2}$$

The electromagnetic torque is expressed by (3):

$$T_e = \frac{3}{2}\cdot\frac{P_n}{2}\cdot\lambda_m'\cdot i_{qs}^{r} = K_t i_{qs}^{r} \tag{3}$$

The PMSM equation of motion is described by (4):

$$T_e - T_L = J_m\,(2/P_n)\,\frac{d}{dt}\omega_r + \beta_m\,(2/P_n)\,\omega_r \tag{4}$$

The PMSM dynamic model in (1)-(4) using the FOC in the synchronous reference frame can be expressed by (5) [18]–[20]:

$$\begin{cases} \dot{\omega}_r = \dfrac{K_t}{J_m} i_{qs}^{r} - \dfrac{\beta_m}{J_m}\omega_r - \dfrac{1}{J_m} T_L \\ \dot{i}_{qs}^{r} = -\dfrac{R_s}{L_{ss}} i_{qs}^{r} - \omega_r i_{ds}^{r} - \dfrac{1}{L_{ss}}\omega_r \lambda_m' + \dfrac{1}{L_{ss}} V_{qs}^{r} \\ \dot{i}_{ds}^{r} = -\dfrac{R_s}{L_{ss}} i_{ds}^{r} + \omega_r i_{qs}^{r} + \dfrac{1}{L_{ss}} V_{ds}^{r} \end{cases} \tag{5}$$

where i_{qs}, i_{ds}, V_{qs}, and V_{ds}, represent the stator currents along with voltages, respectively. R_s & L_{ss} denote the stator resistance along with the stator self-inductance, respectively. J_m, β_m, θ_r, ω_r, as well P_n represent the motor inertia, friction coefficient, the PMSM rotor position angle, PMSM electrical rotor angular speed, as well the number of motor poles, respectively. T_L & T_e denote the load and electromagnetic torques, respectively. $K_t = (3/2)(P/2)\lambda_m'$ represents the torque constant. $x_1 = \omega_r$, $x_2 = i_{qs}$ and $x_3 = i_{ds}$. The parameters of the three-phase PMSM are given in Table 1 [18]–[20].

TABLE 1. PMSM parameters.

Parameter	Symbol	Value
Rated power	P_n	1.2 W
Rated torque	T_e	0.00044 N.m
Rated speed	N_r	35940 rpm
Rated voltage	$V_{L\text{-}L}$	12 V
Rated current	I	0.105 A
Number of poles	P	2
Rotor inertia	J_m	$4.9\text{x}10^{-9}$ kg.m^2
Friction coefficient	β_m	$2\text{x}10^{-6}$N.m/rad/sec
Stator resistance	R_s	75.4 Ω
Voltage constant	λ_m	3474 rpm/V
Torque constant	K_t	0.00275 N.m/A

B. PROBLEM FORMULATION AND CONTROL OBJECTIVE

PMSM can be considered as a nonlinear system, which can be represented in the state forms via considering the uncertain dynamics as expressed by (6) and the lumped uncertainties in (7) & (8) [18]–[20]:

$$\dot{x}(t) = f_n(x) + g_n(x)u + D(x) \tag{6}$$

$$D(x) = \Delta f(x) + \Delta g(x)u + d \tag{7}$$

$$\left\{|\Delta f(x)| < \Delta_f \text{ and } |\Delta g(x)| < \Delta g \right. \tag{8}$$

The states, the nonlinear continuous functions $g(x)$ along with $f(x)$ as well as the control inputs of the PMSM are given by:

$$x(t) = [\,x_1 \quad x_2 \quad x_3\,]^T = [\,\omega_r \quad i_{qs}^{r} \quad i_{ds}^{r}\,]^T \tag{9}$$

$$f_n(x) = \begin{bmatrix} f_\omega \\ f_q \\ f_d \end{bmatrix} = \begin{bmatrix} -(\beta_m/J_m)x_1 \\ -(R_s/L_{ss})x_2 - x_1x_3 + (\lambda_m'/L_{ss})x_1 \\ -(R_s/L_{ss})x_3 + x_1x_2 \end{bmatrix} \tag{10}$$

$$g_n(x) = \begin{bmatrix} g_\omega & 0 & 0 \\ 0 & g_q & 0 \\ 0 & 0 & g_d \end{bmatrix} = \begin{bmatrix} K_t/J_m & 0 & 0 \\ 0 & 1/L_{ss} & 0 \\ 0 & 0 & 1/L_{ss} \end{bmatrix} \tag{11}$$

$$u = [\,i_{qs}^{r*} \quad V_{qs}^{r*} \quad V_{ds}^{r*}\,]^T \tag{12}$$

where $x(t) = [x_1, x_2, \ldots, x_n]^T \in \Re^n$ represents the state vector, meanwhile, $u(t) = [u_1, u_2, \ldots, u_n]^T \in \Re^n$ represents the control input vector, $g(x(t)) \in \Re^{n\times n}$ & $f(x) \in \Re^n$ are nonlinear functions, as well $g(x)$ is invertible. $D(x(t)) \in \Re^n$ represents unknown lumped uncertainties that hold the unidentified modeling errors, $\Delta g(x)$ & $\Delta f(x)$ denote the parameter disparities, which are greater than zero, τ_d represents the exterior disorders, which

includes the load torque disturbance as well as frictional torque.

Nevertheless the PMSM control methods can guarantee the system stability, but they did not take into account the optimal control obstacle. The stability is considered a chief target in the closed-loop control design. The valued control approach must ensure the stability of the closed-loop system. Hence, the design of the optimal control is important practically. Fig. 1 depicts the proposed OAGSTSMC structure for high-dynamic performance PMSM. From the PMSM perturbed nonlinear dynamic model expressed through (6)-(11), the nonlinearities are exist because of the multiplied PMSM rotor speed, the permanent flux term along with the dq stator current terms. The disturbances can be happened because of the nonlinear characteristics of the CRPWM inverter. This can be considered a significant reason of challenging designing a robust control of PMSM. Moreover, the parameters disparities can increase the nonlinearities along with reduce the performance of the system. For designing a superior control for the PMSM, specific factors e.g. the system nonlinearities, parameter variations and extrinsic load disturbances should be eliminated through the attenuation level. Constructively, the entire nonlinear dependence could be intended into the parameter uncertainties (7) as well as the proposed controller can be designed robust adequate to withstand unmodeled dynamics as well as uncertainties. The nonlinear continuous functions $g(x)$ as well as $f(x)$ are considered uncertain along with bounded, the exterior disturbance d is bounded as well unidentified, along with $\Delta gx)$ & $\Delta f(x)$ are unidentified bounded uncertainty. According to these suppositions, the unknown lumped uncertainties $D(x)$ possesses un upper bound $||D(x(t))|| \leq \delta$, as $\delta > 0$. According to (7), the lumped uncertainties $D(x)$ rely on the $u(t)$, which is the control input, parameter disparities along with the exterior disturbance. Thus, exterior disturbances, parameter disparities, along with nonlinearities can be disregarded through designing a robust controller for the PMSM. Therefore, these nonlinearities along with uncertainties must be considered throughout the PMSM controller design. Therefore, this paper presents the OAGSTSMC using actor-critic approach for controlling the PMSM effectively. According to the suggested strategy, the STSMC coefficients are considered as the design control objective and these coefficients are adjusted through online learning of actor-critic neural networks with HDP.

III. STSMC DESIGN

A. THE STANDARD STSMC DESIGN

The STSMC can be designed for permitting the $x(t)$, which is the state vector to track the $x_d(t)$, which is target trajectory as well as the tracking error $e(t)$ approaches zero. This tracking error can be distinct by $e(t) = x_d(t) - x(t)$; whereas, $x(t) = [x, \dot{x}, \ldots, x^{(n-1)}]$ denotes the state vector; as well $x_d(t) = [x_d, \dot{x}_d, \ldots, x_d^{(n-1)}]$ represents the target trajectory vector. The sliding surface can be expressed by (13):

$$s(t) = \left(\frac{\partial}{\partial t}+\lambda\right)^{(n-1)} e = \sum_{l=0}^{n-1} \frac{(n-1)!}{l!(n-l-1)!} \left(\frac{\partial}{\partial t}\right)^{(n-l-1)} \lambda^l e \tag{13}$$

where λ is greater than zero, which states the slope of the sliding surface. SMC can be performed through two phases: the 1st phase is the approaching one in case $s(t) \neq 0$ as well as the 2nd phase is the sliding one once $s(t) = 0$. For guaranteeing the tracking error transition when reaching the sliding one, the adequate condition can be expressed as in (14):

$$\frac{1}{2}\frac{d}{dt}s^2(t) = s(t)\dot{s}(t) \leq \varphi\,|s(t)|\,; \quad \varphi > 0 \tag{14}$$

$$\begin{aligned} \dot{s}(x,t) &= \sum_{l=0}^{n} \frac{(n-1)!}{l!(n-l-1)!} \left(\frac{\partial}{\partial t}\right)^{(n-l-1)} \lambda^l \dot{e} \\ &= e^{(n)} + \gamma_s \end{aligned} \tag{15}$$

where $\gamma_s = \sum_{l=1}^{n} \frac{(n-1)!}{l!(n-l-1)!} \left(\frac{\partial}{\partial t}\right)^{(n-l-1)} \lambda^l \dot{e}$.

The sliding surface derivative can be expressed as (16):

$$\begin{aligned} \dot{s}(x,t) &= \gamma_s + x_d^{(n)} - x^{(n)} \\ &= \gamma_s + x_d^{(n)} - f_n(x) - g_n(x)u - D(x) \end{aligned} \tag{16}$$

In case the system is limited to the sliding surface, such as $s(t) = 0$, it will be limited within the equivalent control reference u_{eq}, which can be acquired via employing the surface variance conditions, e.g., $s(t) = 0$ & $\dot{s}(t) = 0$ [26], [27]. According to (16), without taking into account the model perturbations, the corresponding control law at $\dot{s}(t) = 0$ can be expressed by (17):

$$u_{eq}(t) = \frac{1}{g_n(x)}\left[-f_n(x) + \gamma_s + x_d^{(n)}\right] \tag{17}$$

The switching control law is designed via employing super-twisting technique as in (18):

$$\begin{aligned} u_{st}(t) &= \dot{u}_1 + u_2 = \int_0^t \sigma_1 \mathrm{sgn}(s(x,t))dt \\ &\quad + \sigma_2\,|s(x,t)|^{(1/2)}\,\mathrm{sgn}(s(x,t)) \end{aligned} \tag{18}$$

The STSMC law is acquired via summing (17) & (18) as in (19):

$$\begin{aligned} &u_{STSMC}(t) \\ &= \frac{1}{g_n(x)}\begin{bmatrix} -f_n(x) + \gamma_s + x_d^{(n)} + \int_0^t \sigma_1 \mathrm{sgn}(s(x,t))dt \\ +\sigma_2\,|s(x,t)|^{(1/2)}\,\mathrm{sgn}(s(x,t)) \end{bmatrix} \end{aligned} \tag{19}$$

where $\sigma_1 > 0$, $\sigma_2 > 0$ and $\sigma_1 > \vartheta > \left|\dot{D}(t)\right|$; ϑ denotes the derivative of the uncertainty upper bound as well $\vartheta > 0$.

Since the system has relative degree 1, the second derivative of the sliding surface (16) is given by:

$$\begin{aligned} \ddot{s}(x,t) &= \dot{\gamma}_s + x_d^{(n+1)} - \dot{f}_n(x) - g_n(x)\dot{u} - \dot{D}(x) \\ &= \phi(x,t) - \Gamma(x,t)\dot{u} \end{aligned} \tag{20}$$

where $\phi(x,t) = \dot{\gamma}_s + x_d^{(n+1)} - \dot{f}_n(x) - \dot{g}_n(x)u - \dot{D}$ and $\Gamma(x,t) = g_n(x)$. In order to satisfy the constraint (14) and to ensure the convergence and stability of the system, the control gains σ_1 and σ_2 should be chosen as follows:

$$\begin{cases} \sigma_1 > \dfrac{\rho}{\Gamma_m} \\ \sigma_2 \geq \dfrac{4\rho}{\Gamma_m^2} \cdot \dfrac{\Gamma_M(\sigma_1+\rho)}{\Gamma_m(\sigma_1-\rho)} \\ |\phi \leq \rho|, \quad \rho > 0 \end{cases} \tag{21}$$

where σ_1 and σ_2 are variable controller parameters, ρ is a positive norm bound on the smooth uncertain function ϕ and Γ_m and Γ_M are lower and upper positive bounds on the smooth uncertain function.

B. STABILITY ANALYSIS OF THE STANDARD STSMC

Select a Lyapunov function candidate as indicated in (22):

$$V(t) = \frac{1}{2}s^T s \tag{22}$$

Differentiate $V(t)$ and using (16) will give (23):

$$\begin{aligned} \dot{V}(t) &= s^T \dot{s} \\ &= s^T [\int_0^t \sigma_1 \mathrm{sgn}(s))dt - \sigma_2 |s|^{(1/2)} \mathrm{sgn}(s) + D(t)] \\ &\leq -\sigma_2 \left|s^T\right| |s|^{(1/2)} - \left|s^T\right| \int_0^t \sigma_1 dt + \left|s^T D(t)\right| \\ &\leq -\sigma_2 \left|s^T\right| |s|^{(1/2)} - \left|s^T\right| \int_0^t \sigma_1 dt + \left|s^T\right| \int_0^t \dot{D}(t)dt \end{aligned} \tag{23}$$

Because $\sigma_1 > \vartheta > \left|\dot{D}(t)\right|$, then (23) becomes:

$$\begin{aligned} \dot{V}(t) &\leq -\sigma_2 \left|s^T\right| |s|^{(1/2)} - \left|s_1^T\right| \int_0^t \sigma_1 dt + \left|s_1^T\right| \int_0^t \vartheta dt \\ &= -\sigma_2 \left|s^T\right| |s|^{(1/2)} - \left|s_1^T\right| (\int_0^t \sigma_1 dt - \int_0^t \vartheta dt) \\ &\leq -\sigma_2 \left|s^T\right| |s|^{(1/2)} \leq 0 \end{aligned} \tag{24}$$

As $\dot{V}$ is less than or equal zero, thus, $\dot{V}$ is negative semi-definite, afterwards, the closed-loop system's global asymptotic stability is assured, along with $s(t) \equiv 0$ when $\dot{V} \equiv 0$. Hence, $s(t) = 0$ as well as $\dot{s}(t) = 0$ in a limited time, will ensure the PMSM stability as well as robustness. Proof is accomplished.

C. STSMC DESIGN FOR SPEED AND CURRENT CONTROL OF PMSM

1) SPEED CONTROL DESIGN USING STSMC

In this section, the outer loop super-twisting sliding-mode speed control is deigned based on the standard STSMC which is introduced in previous section.

The derivative of sliding surface for speed loop can be expressed by (25):

$$\begin{aligned} \dot{s}_\omega(x,t) &= \gamma_{s\omega} + \dot{\omega}_r^* - \dot{\omega}_r \\ &= \gamma_{s\omega} + \dot{\omega}_r^* - f_\omega(x) - g_\omega(x)u_{qs}^* - D_\omega \end{aligned} \tag{25}$$

Based on (19), the super-twisting sliding-mode speed control law is designed as:

$$\begin{aligned} & i_{qs}^{r*}(t) \\ &= \frac{1}{g_\omega(x)} \begin{bmatrix} -f_\omega(x) + \gamma_{s\omega} + \dot{\omega}_r^* + \int_0^t \sigma_{1\omega} \mathrm{sgn}(s_\omega(x,t))dt \\ +\sigma_{2\omega} |s_\omega(x,t)|^{(1/2)} \mathrm{sgn}(s_\omega(x,t)) \end{bmatrix} \end{aligned} \tag{26}$$

where $f_\omega = -(\beta_m/J_m)\omega_r$, $g_\omega = K_t/J_m$; $\sigma_{1\omega}$ and $\sigma_{2\omega}$ are the control gains of the super-twisting sliding-mode speed controller. i_{qs}^{r*} is the reference torque current component in q-axis.

2) CURRENT CONTROL DESIGN USING STSMC

Similarly, the inner loop super-twisting sliding-mode current controllers in d-q axes are designed. The reference currents i_{qs}^{r*} and i_{ds}^{r*} remain on their sliding surfaces $s_q(t) = 0$ and $s_d(t) = 0$, by applying the suitable voltage vectors V_{qs}^{r*} and V_{ds}^{r*} at each sampling time. The derivative of sliding surfaces for d-q axis current control loops are given by:

$$\begin{aligned} \dot{s}_q(t) &= \gamma_{sq} + \dot{i}_{qs}^{r*} - \dot{i}_{qs}^{r} \\ &= \gamma_{sq} + \dot{i}_{qs}^{r*} - f_q - g_q V_{qs}^{r*} - D_q \end{aligned} \tag{27}$$

$$\begin{aligned} \dot{s}_d(t) &= \gamma_{sd} + \dot{i}_{ds}^{r*} - \dot{i}_{ds}^{r} \\ &= \gamma_{sd} + \dot{i}_{ds}^{r*} - f_d - g_d V_{ds}^{r*} - D_d \end{aligned} \tag{28}$$

According to (19), the super-twisting sliding-mode control laws are designed as

$$V_{qs}^{r*STSMC}(t) = \frac{1}{g_q} \begin{bmatrix} -f_q + \gamma_{sq} + \dot{i}_{qs}^{r*} + \int_0^t \sigma_{1q} \mathrm{sgn}(s_q(t))dt \\ +\sigma_{2q} |s_q(t)|^{(1/2)} \mathrm{sgn}(s_q(t)) \end{bmatrix} \tag{29}$$

$$V_{ds}^{r*STSMC}(t) = \frac{1}{g_d} \begin{bmatrix} -f_d + \gamma_{sd} + \dot{i}_{ds}^{r*} + \int_0^t \sigma_{1d} \mathrm{sgn}(s_d(t))dt \\ +\sigma_{2q} |s_d(t)|^{(1/2)} \mathrm{sgn}(s_d(t)) \end{bmatrix} \tag{30}$$

where $V_{qs}^{r*STSMC}$ and $V_{ds}^{r*STSMC}$ are the reference command voltages in d-q axis, $f_q = -(R_s/L_{ss})i_{qs}^r - \omega_r i_{ds}^r + (\lambda_m'/L_{ss})\omega_r$, $f_d = -(R_s/L_{ss})i_{ds}^r + \omega_r i_{qs}^r$, $g_q = 1/L_{ss}$, $g_d = 1/L_{ss}$; σ_{1q}, σ_{2q}, σ_{1d} and σ_{2d} are the control gains of the super-twisting sliding-mode current controllers. The stability analysis of the speed and current controllers can be proved like the standard STSMC given in Section III.

It is observed that the STSMC laws (19), (26), (29) and (30) depend on the σ_1, σ_2, λ and the nonlinear functions $f_n(x)$ and $g_n(x)$. Though, the choice of the control gains σ_1 along with σ_2 in the approaching phase needs defining the upper bound of $D(t)$& $\dot{D}(t)$. Moreover, the functions $f_n(x)$ & $g_n(x)$ are not accurately identified beforehand for industrial applications. Also, the sign(s) origins a chattering problem. For enhancing the performance of the standard super-twisting approach by avoiding both the chattering and the constraints on the knowledge of disturbances and uncertainties upper

bounds, an adaptive-gains STSMC (AGSTSMC) is designed as follows.

IV. ADAPTIVE-GAINS SUPER-TWISTING SLIDING-MODE CONTROL (AGSTSMC) DESIGN

The adaptive gains super-twisting sliding-mode control (AGSTSMC) is formulated in the following theorem.

Theorem 1: Consider the control input (18), (19). Suppose the perturbation D is bounded as $D \le \mu\,|s(x,t)|^{(1/2)}$ where, $\mu > 0$ is unidentified. Afterwards, for any initial conditions $x(0)$, $s(0)$, the sliding surface $s = 0$ will be reached in finite time via super-twisting control law in (19) with the adaptive gains in (31) [40]:

$$\begin{cases} \dot{\hat{\sigma}}_{1-AG} = \begin{cases} \xi\sqrt{\dfrac{\alpha}{2}} & \text{if } s \neq 0 \\ 0 & \text{if } s = 0 \end{cases} \\ \dot{\hat{\sigma}}_{2-AG} = \kappa\xi\sqrt{\dfrac{\alpha}{2}} \end{cases} \tag{31}$$

where α, ξ and κ denote arbitrary positive constants.

Proof: Theorem 1 proof is similar to [40], [41].

The STSMC-AG control law in general form is designed as (32) and (33):

$$u^{STSMC-AG} = \frac{1}{g_n(x)}\begin{bmatrix} -f_n(x) + x_d^{(n)} + \int_0^t \hat{\sigma}_{1-AG}\mathrm{sgn}(s(x,t))dt \\ +\hat{\sigma}_{2-AG}\,|s(x,t)|^{(1/2)}\,\mathrm{sgn}(s(x,t)) + \gamma_s \end{bmatrix} \tag{32}$$

$$\begin{cases} \hat{\sigma}_{1-AG} = [\,\hat{\sigma}_{1\omega-AG} \quad \hat{\sigma}_{1q-AG} \quad \hat{\sigma}_{1d-AG}\,] \\ \hat{\sigma}_{2-AG} = [\,\hat{\sigma}_{2\omega-AG} \quad \hat{\sigma}_{2q-AG} \quad \hat{\sigma}_{2d-AG}\,] \end{cases} \tag{33}$$

where $f_n(x) = [f_\omega(x), f_q(x), f_d(x)]$, $g_n(x) = [g_\omega(x), g_q(x), g_d(x)]$, $s(x,t) = [s_\omega(x,t), s_q(x,t), s_d(x,t)]$, $\gamma_s = [\gamma_\omega, \gamma_q, \gamma_d]$, $x(t) = [\omega_r, i_{qs}^r, i_{ds}^r]$ and $\dot{x}_d(t) = [\dot{\omega}_r, \dot{i}_{qs}^r, \dot{i}_{ds}^r]$. $\hat{\sigma}_{1-AG}(t)$ and $\hat{\sigma}_{2-AG}(t)$ are the adaptive control gains, and the outputs of the speed and current AGSTSMC controllers of the PMSM drive system are $u^{STSMC-AG}(t) = [i_{qs}^{r*STSMC-AG}, V_{qs}^{r*STSMC-AG}, V_{ds}^{r*STSMC-AG}]$.

In this case, the AGSTSMC control law will derive the system's (1) trajectory to the ideal 2-sliding mode, i.e. $s(t) = \dot{s}(t) = 0$ in finite time. However, the adaptive gains $\hat{\sigma}_{1-AG}(t)$ and $\hat{\sigma}_{2-AG}(t)$ can be overestimated. Therefore, an optimal online gain tuning scheme based on actor-critic neural network algorithm via the HDP technique is proposed for fulfilling the PMSM drive system robustness as given in the following section.

V. THE DESIGN OF THE OAGSTSMC

The optimal online gain tuning approach in this section is suggested to enhance the AGSTSMC control approach according to the optimal dynamic response for the PMSM. In the design of the OAGSTSMC scheme, the ACNN-HDP algorithm, as an optimal adaptive mechanism tuner, is adopted to optimize the AGSTSMC coefficients. According to the proposed strategy, these coefficients are considered as the design control objective and the ACNN-HDP tuner adjusts these coefficients through online learning of actor-critic neural networks. The structure of the proposed OAGSTSMC for the PMSM based on the ACNN-HDP tuner is shown in Fig. 1. The ACNN-HDP algorithm produces the commands $\hat{\Xi}_{1oac}$ and $\hat{\Xi}_{2oac}$ to tune and optimize the gains of the proposed control scheme. The OAGSTSMC control algorithm is designed as:

$$u^{STSMC-OAG} = \frac{1}{g_n(x)}\begin{bmatrix} -f_n(x) + x_d^{(n)} + \int_0^t \hat{\Xi}_1\mathrm{sgn}(s(x,t))dt \\ +\hat{\Xi}_2\,|s(x,t)|^{(1/2)}\,\mathrm{sgn}(s(x,t)) + \gamma_s \end{bmatrix} \tag{34}$$

$$\hat{\Xi}_1(t) = \hat{\sigma}_{1-AG}(t) + \hat{\Xi}_{1oac}(t) \tag{35}$$

$$\hat{\Xi}_2(t) = \hat{\sigma}_{2-AG}(t) + \hat{\Xi}_{2oac}(t) \tag{36}$$

$$\begin{cases} \hat{\Xi}_{1oac} = [\,\hat{\Xi}_{1oac-\omega} \quad \hat{\Xi}_{1oac-q} \quad \hat{\Xi}_{1oac-d}\,] \\ \hat{\Xi}_{2oac} = [\,\hat{\Xi}_{2oac-\omega} \quad \hat{\Xi}_{2oac-q} \quad \hat{\Xi}_{2oac-d}\,] \end{cases} \tag{37}$$

where $\hat{\Xi}_{1oac}$ and $\hat{\Xi}_{2oac}$ denote the optimal adaptive gains estimated by the ACNN-HDP optimal tuner for the PMSM speed and current controllers.

Through the following sections, the implementation process of optimal adaptive gains tuning based on the ACNN-HDP is introduced.

A. DIRECT HDP CONTROL ALGORITHM

The direct HDP structured in Fig. 2, is a learning algorithm for adapting the critic and the action components. These two components can be implemented using any kind of differentiable function approximator. The most widely used value function approximators in practical applications are neural networks [73], [75]. Let us express the utility function in the ACNN-HDP at instant t as:

$$r(t) = f_r(t)C_r f_r^T(t) \tag{38}$$

where $f_r(t) = [z^T(t), \Xi_{ac}^T(t)]$, $z(t) = [\,s(t) \;\; x(t)\,]$, $s(t) = [\,s_\omega \;\; s_q \;\; s_d\,]^T$, $x(t) = [\,\omega_r \;\; i_{qs}^r \;\; i_{ds}^r\,]^T$ and $C_r(t)$ is a positive-definite diagonal matrix. The vector $z(t)$ includes the sliding surfaces $s(t)$ and state $x(t)$ that can be applied to the actor NN. The reinforcement function $r(t)$ is required to be bounded semi-definite function of the vector $z(t)$ and control inputs.

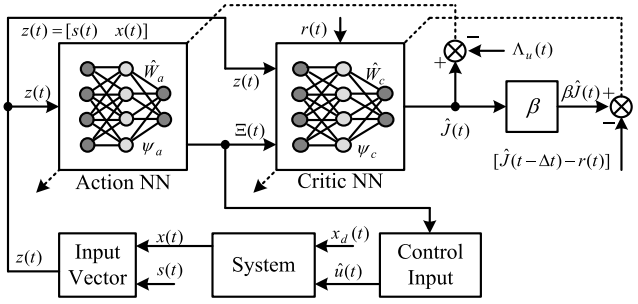

FIGURE 2. Implementation process of the direct HDP.

A cost-to-go function is adopted as:

$$J(z(t),\, \Xi_{ac}(t)) = \sum_{t=0}^{\infty} \beta r(z(t+\Delta t), \Xi_{ac}(t+\Delta t)) \quad (39)$$

where $0 < \beta < 1$ denotes a discount factor for the infinite horizon problem and $\Xi_{ac} = [\ \Xi_{1ac} \quad \Xi_{2ac}\ ]$.

The optimal cost function $J^*(z(t))$ is the solution of (39) which satisfies the following HJB equation:

$$J^*(z(t)) = \min_{\Xi_{ac}(t)} \left(r(z(t),\, \Xi_{ac}(t)) + \beta J^*(z(t+\Delta t)) \right) \quad (40)$$

The ACNN-HDP technique can be employed as policy iteration for solving the HJB equation (40). Moreover, $J^*(z(t))$ can be approximated via $\hat{J}(z(t))$, which denotes the critic neural network output. The critic NN inputs are $z(t)$ and the optimal adaptive gains $\Xi_{ac}(t)$ which are estimated by the actor neural network.

B. CRITIC NEURAL NETWORK

The critic neural network is used to approximate the cost function J and it uses the output of the actor neural network as one of its inputs. The critic network inputs are $z(t) = [\ s(t) \quad x(t)\ ]$ and the optimal adaptive gains $\Xi_{ac}(t)$ which are estimated by the actor neural network. Define the error function for the backpropagation of the critic network as:

$$e_c(t) = \beta \hat{J}(t) - [\hat{J}(t-\Delta t) - r(t)] \quad (41)$$

For the critic NN weights update, a target function can be minimized expressed by (42):

$$\min_{\varpi_c(t)} E_c(t) = \min_{\varpi_c(t)} \frac{1}{2} e_c^T(t) e_c(t) \quad (42)$$

Fig. 3 depicts the architecture of the critic, which is a multi-layer perceptron (MLP) network comprises an input layer, a hidden layer and an output layer. The activation function for critic neural network is chosen as:

$$\psi_c(t) = \frac{1 - e^{-t}}{1 + e^{-t}} \quad (43)$$

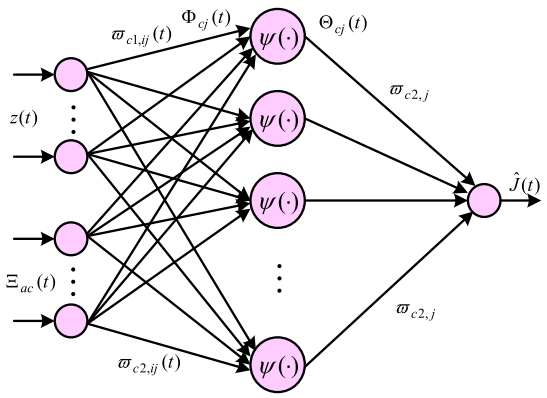

FIGURE 3. Structure of the critic neural network model.

The critic neural network signal propagation and the basic functions can be expressed by:

$$\Phi_{cj}(t) = \sum_{i=1}^{n} z_i(t) \varpi_{c1,ij}(t) + \sum_{i=1}^{m} \Xi_{aci}(t) \varpi_{c2,ij}(t) \quad j = 1, \ldots, N_{ch} \quad (44)$$

$$\Theta_{cj}(t) = \psi_c(\Phi_{cj}(t)) = \frac{1 - e^{-\Phi_{cj}(t)}}{1 + e^{-\Phi_{cj}(t)}} \quad j = 1, \ldots, N_{ch} \quad (45)$$

where $\varpi_{c1,ij}(t)$ and $\varpi_{c2,ij}(t)$ are the weights of the critic neural network, n and m are the number of inputs and outputs of the actor neural network, respectively. The critic neural network has $N_{ci} = (n+m)$ input nodes, N_{ch} hidden nodes and one output node. $\Phi_{cj}(t)$ along with $\Theta_{cj}(t)$ denote the input and output of the jth hidden node, respectively. The approximated cost function can be expressed by (46):

$$\hat{J}(t) = \sum_{j=1}^{N_{ch}} \varpi_{c2,j} \Theta_{cj}(t) \quad (46)$$

The weight update law from the hidden through the output layer for the critic neural network using gradient-descent adaptation is given by:

$$\begin{aligned} \Delta W_c(t) &= -\eta_c(t) \frac{\partial E_c(t)}{\partial W_c(t)} \\ &= -\eta_c(t) \frac{\partial E_c(t)}{\partial \hat{J}(t)} \frac{\partial \hat{J}(t)}{\partial W_c(t)} \\ &= -\eta_c(t) \beta e_c(t) \Theta_c(t) \quad (47) \\ W_c(t+\Delta t) &= W_c(t) + \Delta W_c(t) \quad (48) \end{aligned}$$

where $\eta_c(t) > 0$ represents the critic NN learning at time t that regularly decays with time to an insignificant value and W_c denotes the weight vectors form hidden to output layer in the critic NN. The online learning algorithms based gradient-descent method for the critic NN are given in the Appendix.

C. ACTOR NEURAL NETWORK

The action component will be represented by an actor neural network and its main goal is to generate control policy. Similar to the critic neural network, an MLP structure with one hidden layer is used as depicted in Fig. 4. The actor NN is adopted for estimating the optimal adaptive gains of the STSMC. The inputs to the actor network is $z(t)$. The error function for the actor neural network backpropagation is defined by (49):

$$e_a(t) = \hat{J}(t) - \Lambda_u \quad (49)$$

where Λ_u is the desired ultimate target value of the entire cost-to-go as well as can be regularly set to 0, which means the accomplishment learning implementation for all t. The actor NN target function is identified via (50):

$$\min_{\varpi_a(t)} E_a(t) = \min_{\varpi_a(t)} \frac{1}{2} e_a^T(t) e_a(t) \quad (50)$$

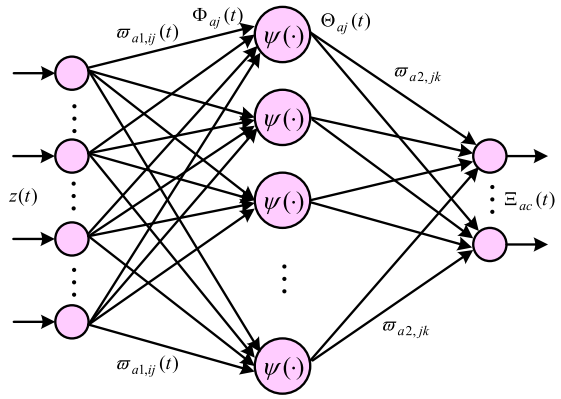

FIGURE 4. Structure of the actor neural network model.

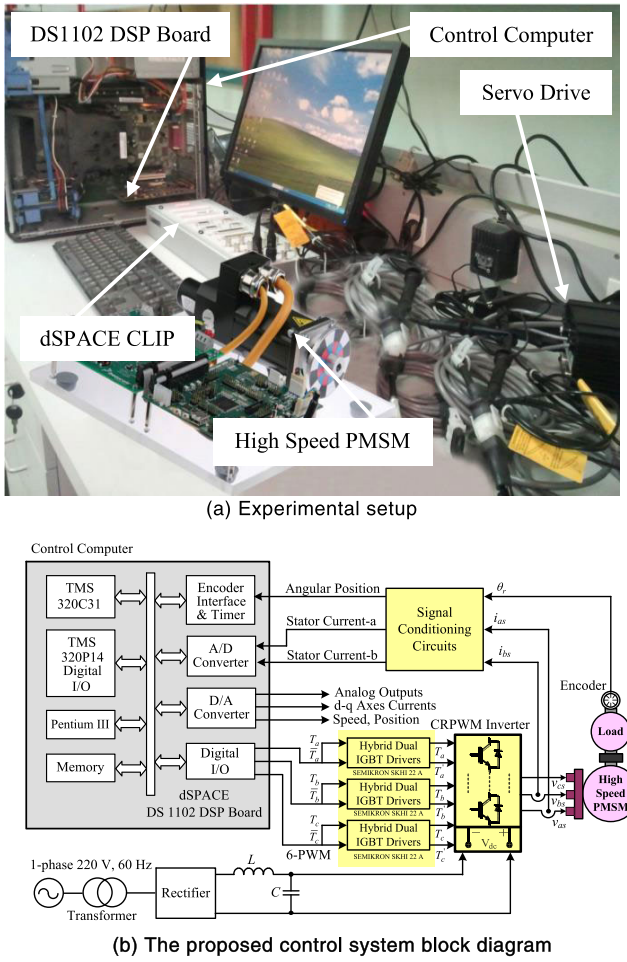

FIGURE 5. The whole developed DSP-based high-speed PMSM schematic diagram.

Similarly, the signal propagation and the basic functions of the actor neural network are represented by:

$$\Phi_{aj}(t) = \sum_{i=1}^{N_{ai}} z_i(t)\varpi_{a1,ij}(t), \quad j = 1, \ldots, N_{ah} \tag{51}$$

TABLE 2. Actor-critic neural networks learning parameters.

Parameter	Definition	Value
$\eta_c(0)$	critic NN initial learning rate	0.20
$\eta_a(0)$	actor NN initial learning rate	0.20
$\eta_c(\infty)$	critic NN final learning rate	0.005
$\eta_a(\infty)$	actor NN final learning rate	0.005
N_{ch}	critic NN hidden nodes	11
N_{ah}	actor NN hidden nodes	9
N_{ao}	actor NN output nodes	3
β	discount factor	0.85
T_c	critic NN tolerance error	10^{-4}
T_a	actor NN tolerance error	10^{-4}
n_c	critic NN internal cycles	100
n_a	actor NN internal cycles	70

$$\Theta_{aj}(t) = \psi_a(\Phi_{aj}(t)) = \frac{1 - e^{-\Phi_{aj}(t)}}{1 + e^{-\Phi_{aj}(t)}}, \quad j = 1, \ldots, N_{ah} \tag{52}$$

$$\Omega_{ak}(t) = \sum_{i=1}^{N_{ai}} \varpi_{a2,jk}(t)\Theta_{aj}(t), \quad k = 1, \ldots, N_{ao} \tag{53}$$

$$\Xi_{ack}(t) = \psi_a(\Omega_{ak}(t)) = \frac{1 - e^{-\Omega_{ak}(t)}}{1 + e^{-\Omega_{ak}(t)}}, \quad k = 1, \ldots, N_{ao} \tag{54}$$

where $\varpi_{a1,ij}$ and $\varpi_{a2,jk}$ are the weights of the actor neural network. The actor neural network has N_{ai} input nodes, N_{ah} hidden nodes and N_{ao} output nodes. $\Phi_{aj}(t)$ along with $\Theta_{aj}(t)$ denote the input and output of the jth hidden node, respectively. $\Omega_{ak}(t)$ & $\Xi_{ack}(t)$ represent the input along with the kth output node, respectively. The ψ_a(t) is the activation function for actor neural network and is chosen as for the critic neural network (43). The estimated optimal adaptive gains via ACNN-HDP optimal tuner are given by:

$$\hat{\Xi}_{oac}(t) = \frac{1 - e^{-\Omega_a(t)}}{1 + e^{-\Omega_a(t)}} \tag{55}$$

$$\hat{\Xi}_{oac}(t) = [\, \hat{\Xi}_{1oac}(t) \quad \hat{\Xi}_{2oac}(t) \,] \tag{56}$$

The weight update law for the actor neural network using gradient-descent adaptation can be expressed as:

$$\begin{aligned} \Delta W_a(t) &= -\eta_a(t)\frac{\partial E_a(t)}{\partial W_a(t)} \\ &= -\eta_a(t)\frac{\partial E_c(t)}{\partial \hat{J}(t)}\frac{\partial \hat{J}(t)}{\partial \Xi(t)}\frac{\partial \Xi(t)}{\partial W_c(t)} \\ &= -\eta_a(t)e_a(t)W_c(t)[(1 - \Xi^2(t))/2]\Theta_a(t) \\ &\quad \times \left[W_a(t)[(1 - \Theta_c^2(t))/2]W_{a1}(t)\right] \end{aligned} \tag{57}$$

$$W_a(t + \Delta t) = W_a(t) + \Delta W_a(t) \tag{58}$$

where $\eta_a(t) > 0$ is the actor neural network learning at instant t that regularly decays with time to an insignificant value and W_a denotes the weight vectors through the actor network. The online learning algorithms details based gradient-descent method for the actor neural network is given in the Appendix.

D. CONVERGENCE ANALYSES

The main target of this section is to afford a convergence bound for the online learning utilizing Lyapunov stability approach to demonstrate that the actor and critic NNs weight

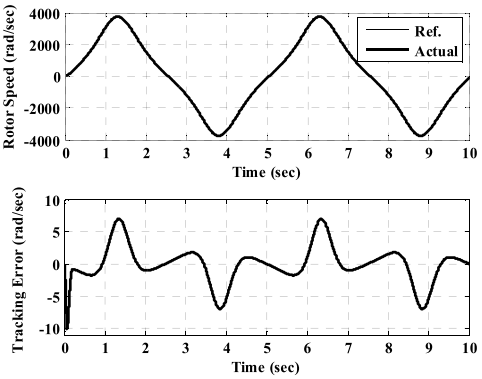

FIGURE 6. Simulation results of the PMSM dynamic response using PID without external disturbance.

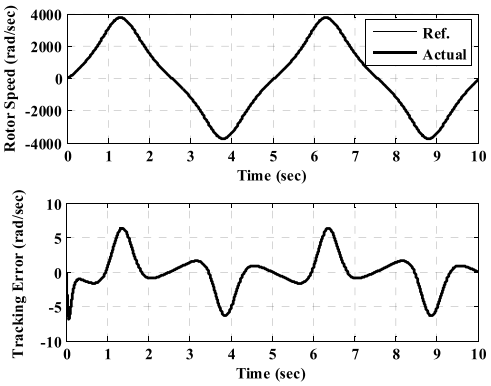

FIGURE 7. Simulation results of the PMSM dynamic response using SMC without external disturbance.

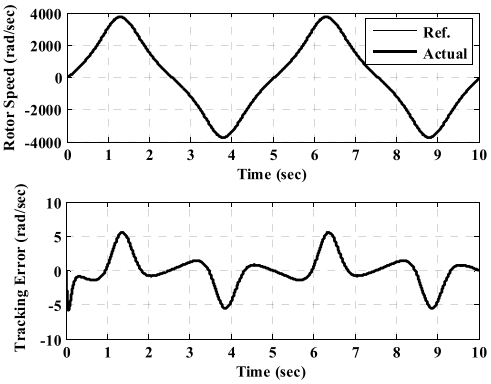

FIGURE 8. Simulation results of the PMSM dynamic response using STSMC without external disturbance.

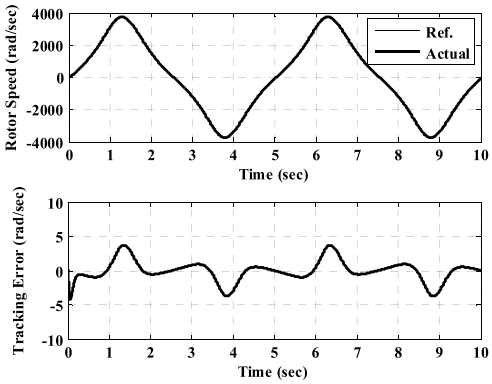

FIGURE 9. Simulation results of the PMSM dynamic response using ASTSMC without external disturbance.

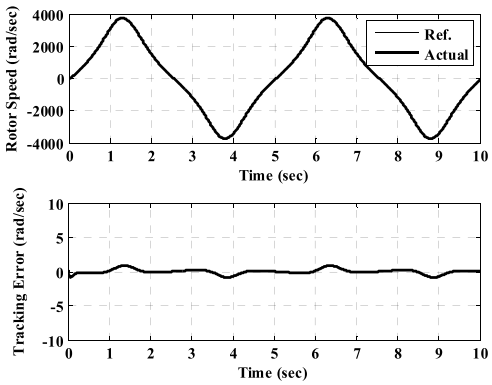

FIGURE 10. Simulation results of the PMSM dynamic response using OAGSTSMC without external disturbance.

estimation errors are uniformly ultimately bounded (UUB). In [72], it was shown that if the input-to-hidden layer weights $\varpi_{c1,ij}(t)$ and $\varpi_{a1,ij}(t)$ are selected initially random and preserved constant as well as if the number of hidden layer neurons is adequately large, afterwards the NN approximation error can be made arbitrarily small. Thus, only the weights of the output layer $\varpi_{c2,j}(t)$ and $\varpi_{a2,jk}(t)$ are suggested to be updated throughout learning. So, from now these weights are denoted by W_c and W_a on the manuscript. As a result, the approximated cost function in (46) can be expressed by (59):

$$\hat{J}(t) = \hat{W}_c^T(t)\Theta_c(t) \tag{59}$$

Correspondingly, $\hat{\Xi}_{ac}(t)$ in (55) can be expressed in a matrix form as in (60):

$$\hat{\Xi}_{ac}(t) = \hat{W}_a^T(t)\Theta_a(t) \tag{60}$$

Substituting (41), (46) and (47) into (48), the weights of the critic neural network can be estimated by (61):

$$\begin{aligned}\hat{W}_c(t+\Delta t) &= \hat{W}_c^T(t) - \eta_c(t)\beta e_c(t)\Theta_c(t)\\ &= \hat{W}_c^T(t) - \eta_c(t)\\ &\quad\times\beta\left(\beta\hat{J}(t) - [\hat{J}(t-\Delta t) - r(t)]\right)\Theta_c(t)\\ &= \hat{W}_c^T(t) - \eta_c(t)\beta\Theta_c(t)\left[\beta\hat{W}_c^T(t)\,\Theta_c(t)\right.\\ &\quad\left.+ r(t) - \hat{W}_c(t-\Delta t)\Theta_c(t-\Delta t)\right]^T\end{aligned} \tag{61}$$

Similarly, the actor neural network weights are estimated based on (58) along with (49), (53) and (57) as:

$$\begin{aligned}\hat{W}_a(t+\Delta t) &= \hat{W}_a^T(t) - \eta_a(t)e_a(t)\\ &\quad\left[\hat{W}_c^T(t)[(1-\Theta_c^2(t))/2]\hat{\varpi}_{c1,ij}(t)\right]\Theta_a(t)\end{aligned}$$

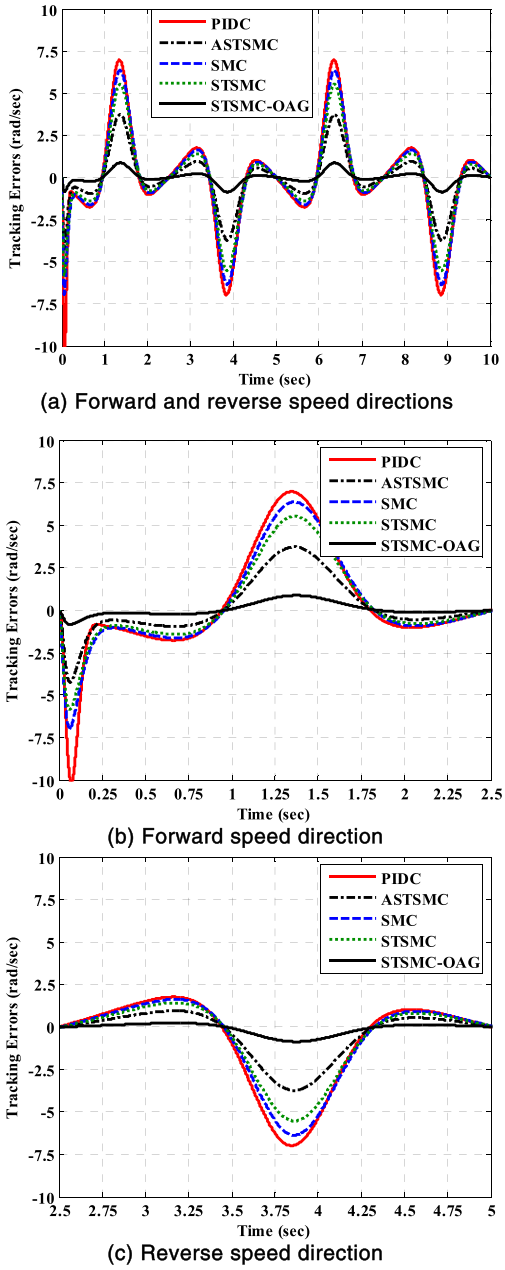

FIGURE 11. Simulation results of the PMSM rotor speed tracking error performance using different control schemes.

$$= \hat{W}_a^T(t) - \eta_a(t)\,\Theta_a(t) \times [\hat{W}_c^T(t)G_{jk}(t)][\hat{W}_c^T(t)\Theta_c(t)]^T \quad (62)$$

where, $G_{jk}(t)$ represents a matrix of $N_{ch} \times$ n dimension, as well as its elements are represented by (63):

$$G_{jk}(t) = \frac{1}{2}[1 - \Theta_c^2(t)]\hat{\varpi}_{cj,m+k}(t) \quad j = 1, \ldots, N_{ch} \quad k = 1 \ldots, m \quad (63)$$

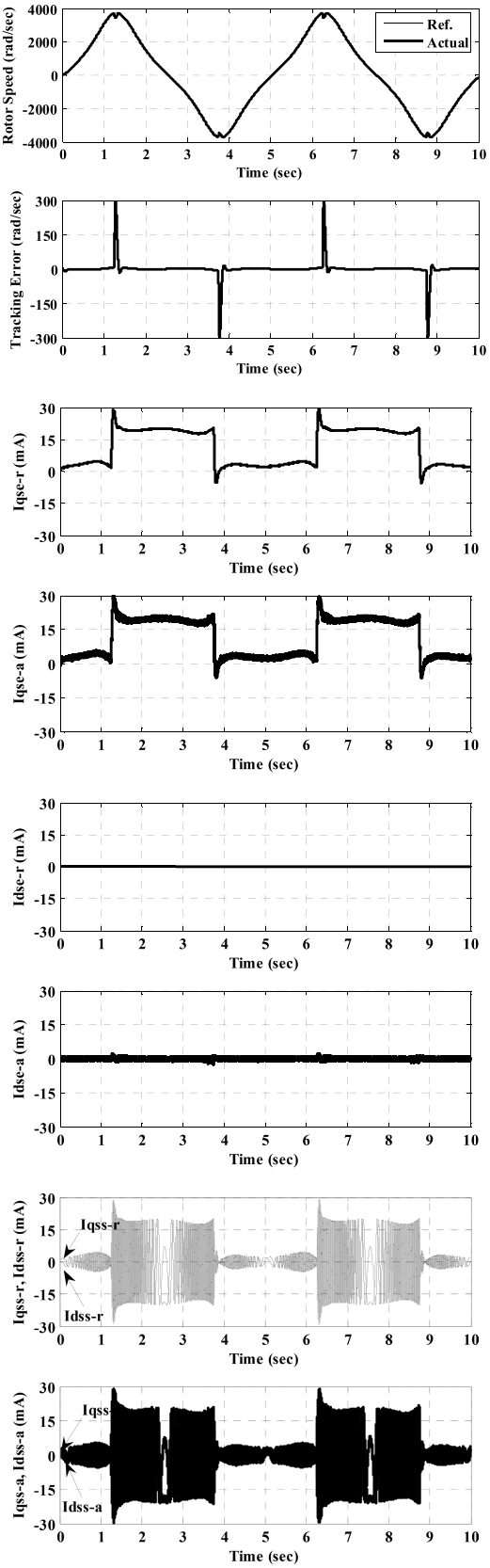

FIGURE 12. Simulation results of the PMSM dynamic response using PID scheme.

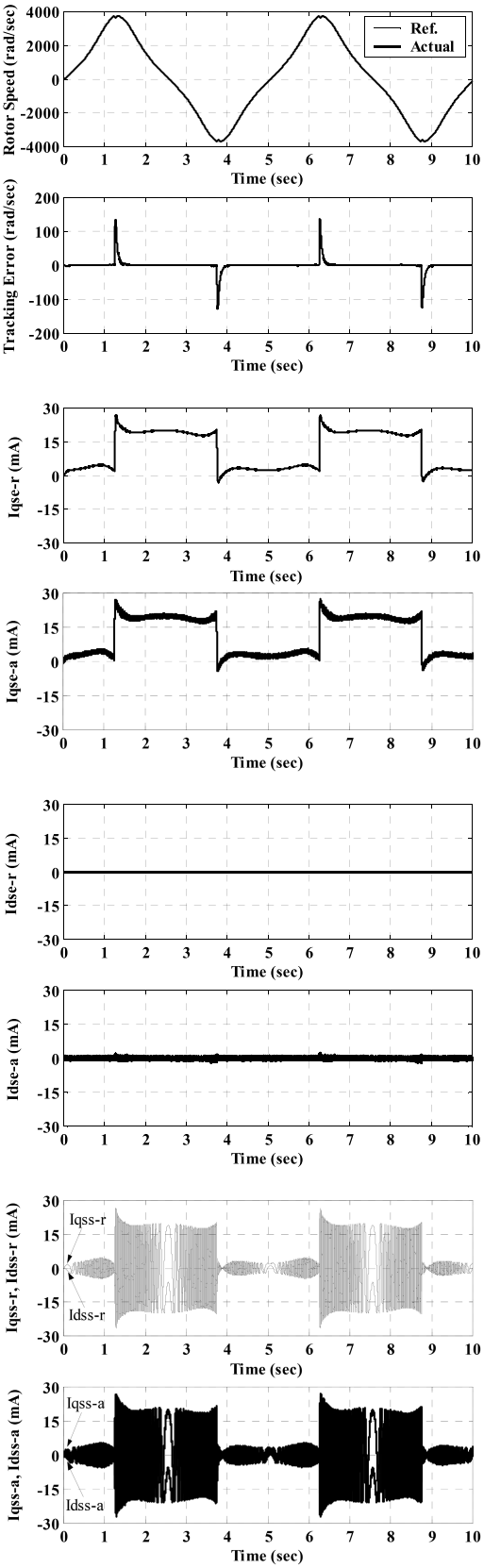

FIGURE 13. Simulation results of the PMSM dynamic response using SMC.

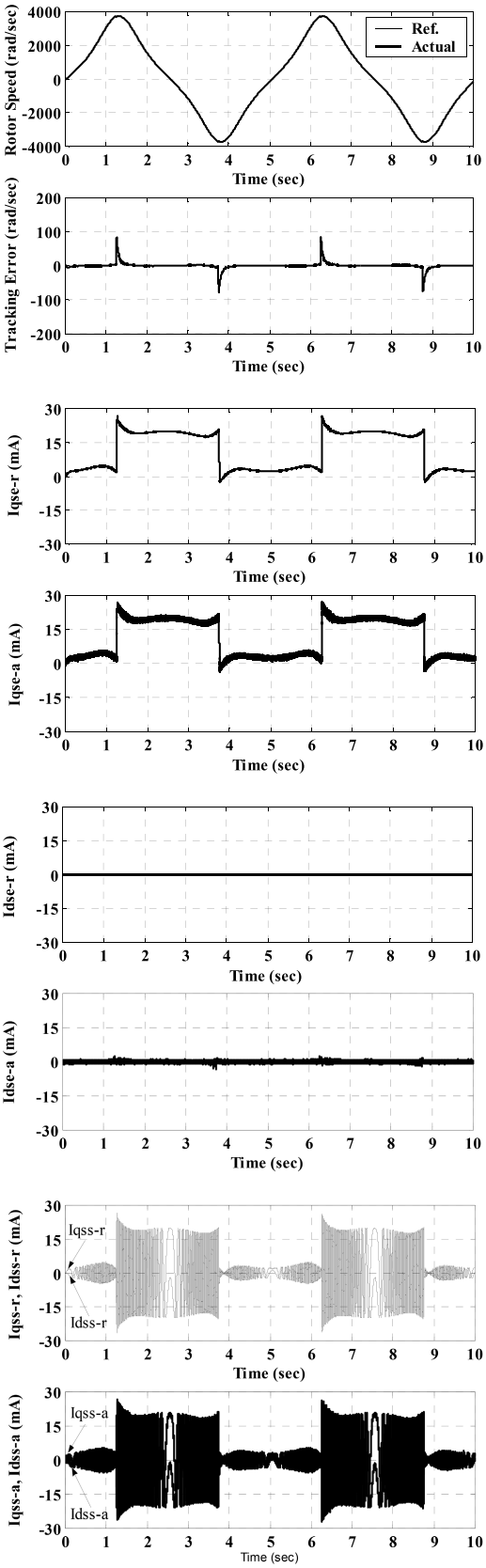

FIGURE 14. Simulation results of the PMSM dynamic response using STSMC scheme.

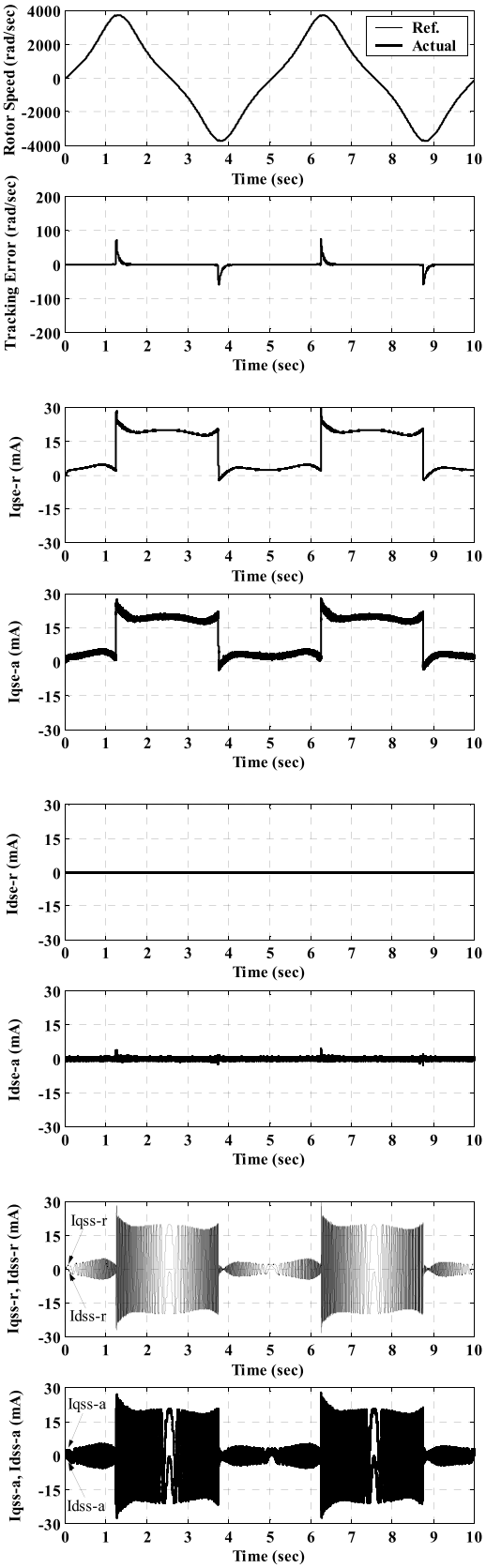

FIGURE 15. Simulation results of the PMSM dynamic performance using ASTSMC scheme.

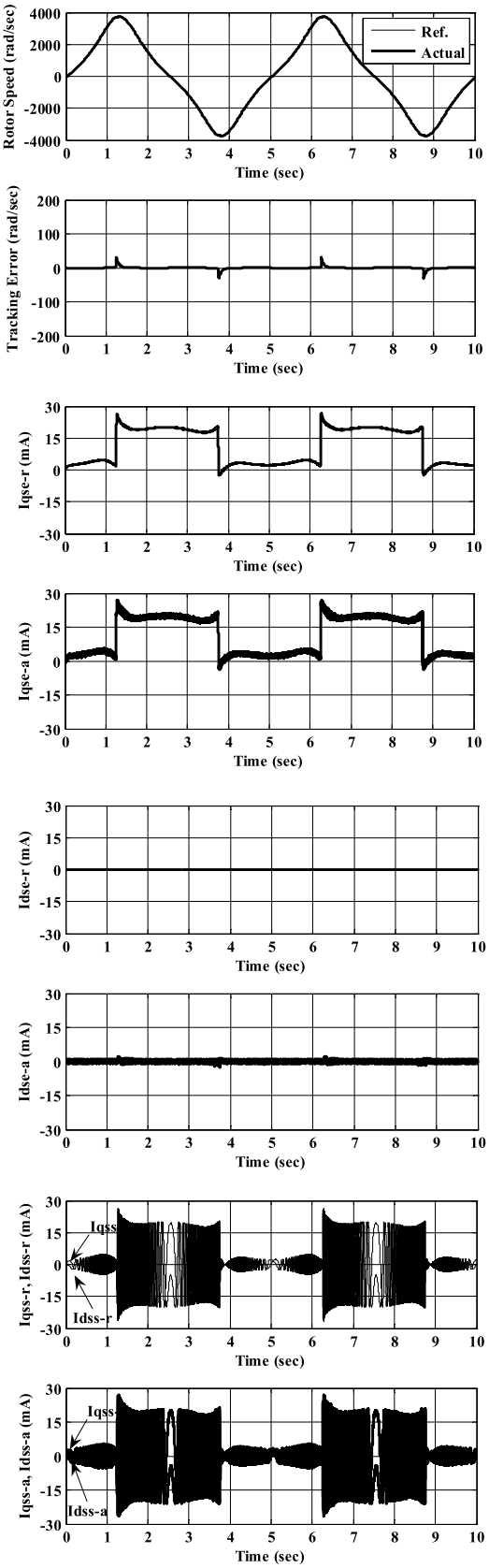

FIGURE 16. Simulation validation results of the PMSM dynamic response using OAGSTSMC scheme.

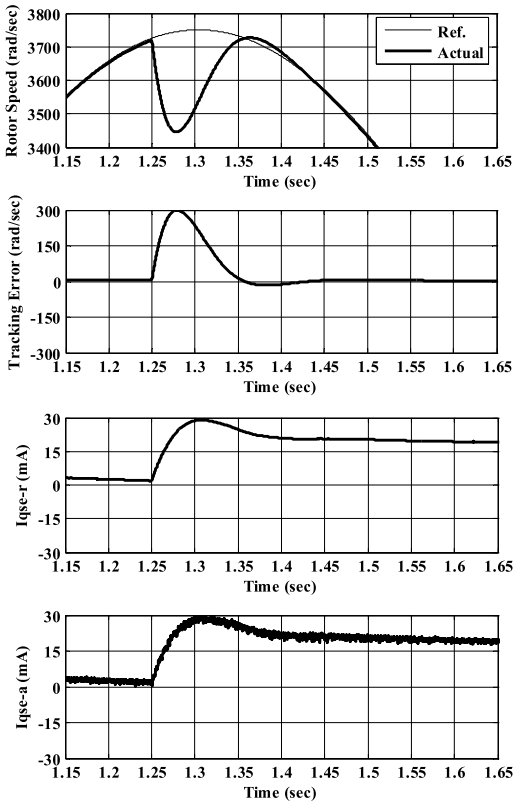

FIGURE 17. Enlarge simulation validation results of the load regulation performance for the PMSM using PID scheme.

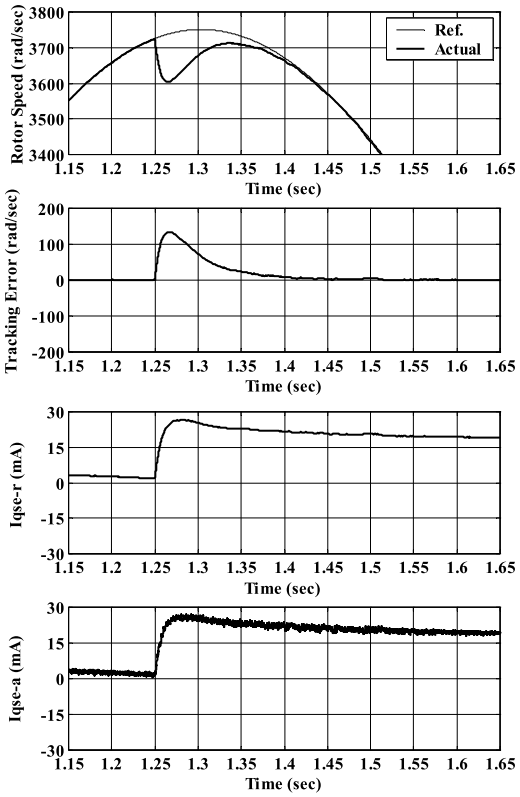

FIGURE 18. Enlarge simulation validation results of the load regulation response for the PMSM using SMC scheme.

Let the optimal weights of the critic along with actor NNs W_c^* and W_a^*, respectively, are represented by:

$$W_c^* = \arg\min_{\hat{W}_c} \left\| \beta \hat{J}(t) - [\hat{J}(t-\Delta t) - r(t)] \right\| \quad (64)$$

$$W_a^* = \arg\min_{\hat{W}_a} \left\| \hat{J}(t) \right\| \quad (65)$$

where $||\cdot||$ represents the 2-norm.

Consider the weight estimation errors for critic along with actor neural networks is defined as $\tilde{W} = (\hat{W} - W^*)$. Then, the weight update laws in (47) and (57) for both actor along with critic neural networks define the dynamic system of the estimation errors and can be expressed by:

$$\tilde{W}_c(t+\Delta t) = \tilde{W}_c(t) - h(\hat{W}_c(t), \hat{W}_c(t-\Delta t), \Theta_c(t), \Theta_c(t-\Delta t)) \quad (66)$$

$$\tilde{W}_a(t+\Delta t) = \tilde{W}_a(t) - h(\hat{W}_a(t), \hat{W}_a(t-\Delta t), \Theta_a(t), \Theta_a(t-\Delta t)) \quad (67)$$

Assumption 1: The critic along with action neural network weights and their activation functions are assumed to be bounded, i.e., $\left\|\hat{W}_a\right\| \le W_{aM}$, $\left\|\hat{W}_c\right\| \le W_{cM}$, $\left\|W_a^*\right\| \le W_{aM}$, $\left\|W_c^*\right\| \le W_{cM}$, $\|\Theta_a\| \le \Theta_{aM}$, $\|\Theta_c\| \le \Theta_{cM}$, $\|r\| \le r_M$ and $\|G\| \le G_M$.

Theorem 2: Consider the output of the critic neural network is given as (59) as well as the critic neural network weights update based on (61), the actor neural network weights update according to (62) using the gradient-descent algorithm. The reinforcement signal is bounded within $0 \le r(t) \le 1$. Afterwards, the errors between the optimal weights W_c^*, W_a^* along with their estimates $\hat{W}_c(t)$, $\hat{W}_a(t)$ denote UUB, respectively, if Assumption 1 and the following conditions are fulfilled:

$$\begin{cases} \eta_c < \dfrac{1}{\beta^2 \|\Theta_c(t)\|^2} \\ \eta_a < \dfrac{1}{\|\Theta_a(t)\|^2} \\ 1/\sqrt{2} < \beta < 1 \end{cases} \quad (68)$$

Proof of Theorem 2: See the Appendix.

The stability analysis of (66) and (67) will be studied to verify the asymptotic performance of the weight estimation errors $\tilde{W}_c$ along with $\tilde{W}_a$. The details of the stability analysis are given in the Appendix by introducing Lemma 1 and Lemma 2 which will be used in Theorem 2 proof.

Remark: In the above sections for different controllers' design, it is observed that the super-twisting sliding-mode control laws (19), (26), (29), (30), (32) and (34) depend on the nonlinear functions $f(x)$ and $g(x)$, which are not accurately identified beforehand for industrial applications. For enhancing the performance of the control system by avoiding the constraints on the knowledge of disturbances and uncertainties upper bounds, an adaptive neural identifier may be used to

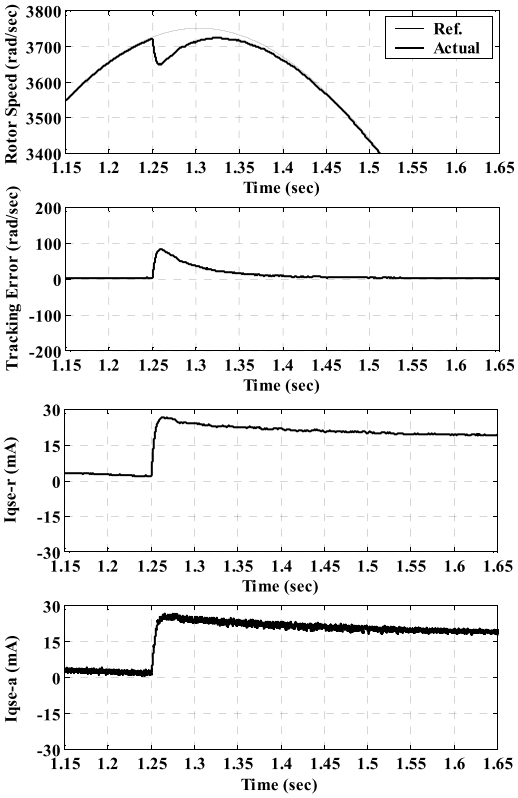

FIGURE 19. Enlarge simulation validation results of the load regulation performance for the PMSM using STSMC scheme.

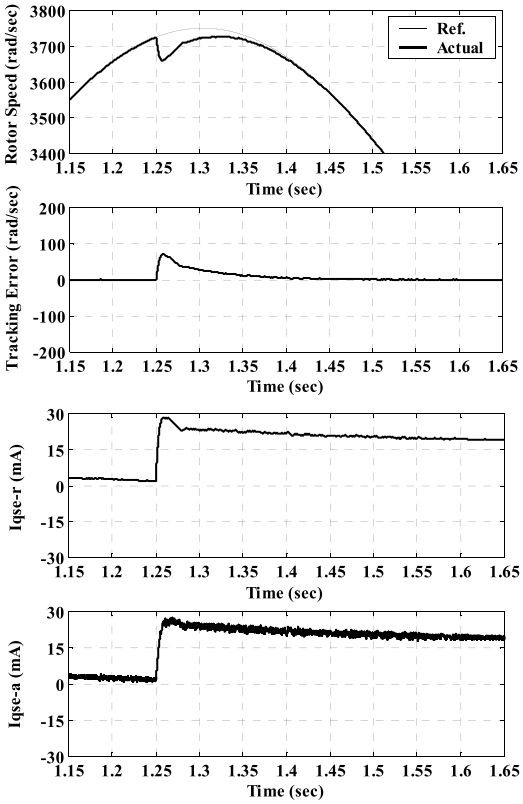

FIGURE 20. Enlarge simulation results of the load regulation performance for the PMSM using ASTSMC scheme.

approximate $f(x)$ and $g(x)$. The control scheme configuration will be actor-critic-identifier structure. In our future research, the actor-critic-identifier structure will be used for online tuning the super-twisting sliding-mode control gains and identify the nonlinear functions $f(x)$ and $g(x)$ to enhance the PMSM dynamic performance.

VI. VALIDATION RESULTS

Firstly, the simulation on the PMSM is conducted to verify the effectiveness of the proposed online OAGSTSMC scheme compared with the PID, SMC, STSMC and ASTSMC control schemes. Then, the experimentation tests are implemented for endorsing the proposed controllers' design validity. The simulation tests are performed in MATLAB according to the control scheme established through Figs. (1)-(4) while the experimental tests are implemented through the experimental setup depicted in Fig. 5 [18]–[20].

A. EXPERIMENTAL SETUP

Fig. 5 depicts the block diagram of the proposed control scheme for the high speed PMSM. For implementing the control operation, a dSPACE DS1102 with TMS320P14 along with TMS320C31 DSPs are employed. The control boards have numerous I/O ports (PIO, ADC, DAC, along with encoder interface) for acquiring the measured signals as well as send the accurate control actions. The inverter PWM signals are produced via a carrier frequency (15 kHz). The sampling time for the current control loops is set to 0.2ms. While the speed control loop operates at a sampling time of 1msec.

B. SELECTION OF ACTOR AND CRITIC NNS

The appropriate actor and critic NNs are selected as follows. First, in order to evaluate the effectiveness of the learning control algorithms in simulation and implementation, the parameters of the actor-critic neural networks are given in Table 2. The OAGSTSMC based on actor-critic NNs via HDP are trained online based on two stop criterions. The training of the actor and critic NNs is accomplished utilizing their internal cycles n_a and n_c, respectively. At each time step, the update of W_a and W_c weights is carried out at most n_a and n_c times, respectively, or stopped once the tolerance error T_a and T_c have been reached.

C. SIMULATION RESULTS

Numerical simulations are carried out for investigating the efficacy of the proposed OAGSTSMC with actor-critic identifier for optimal adaptive gains applied to the PMSM. The MATLAB simulation results of applying the OAGSTSMC to the PMSM are analyzed based on the control system presented in Fig. 1 to Fig. 4. In addition, the PID, SMC, STSMC and ASTSMC control approaches are applied to the same

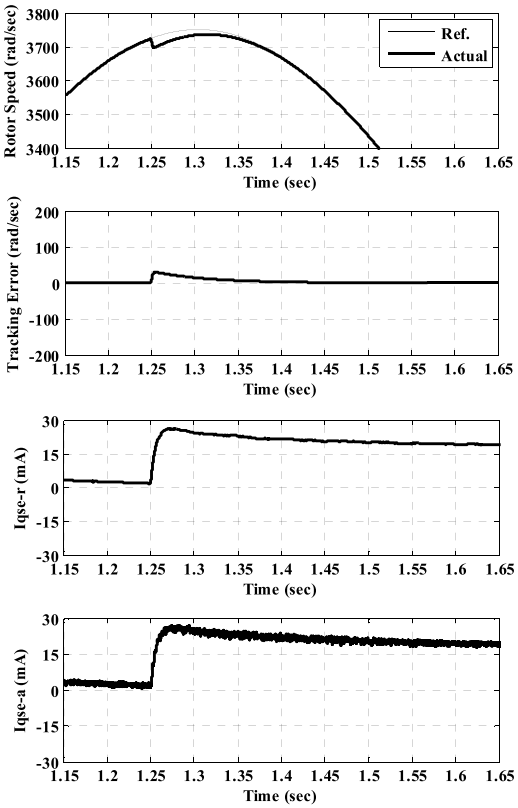

FIGURE 21. Enlarge simulation results of the load regulation performance for the PMSM drive using OAGSTSMC scheme.

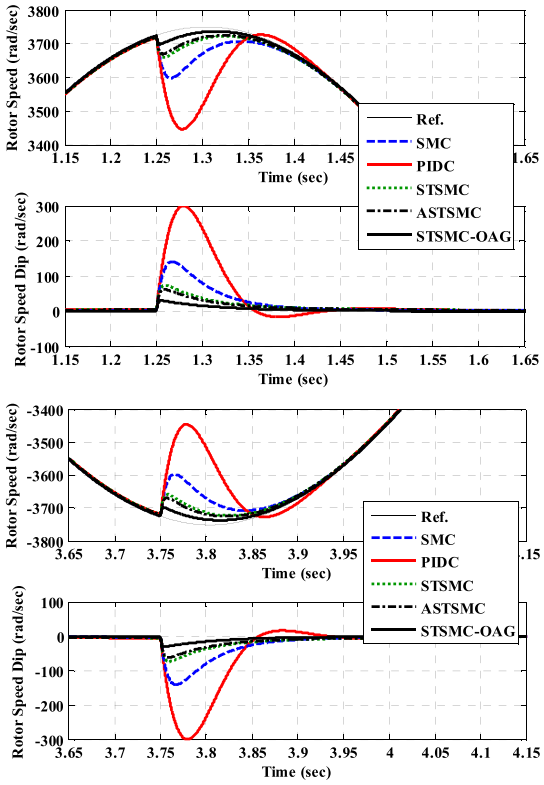

FIGURE 22. Enlarge simulation results of the external disturbance regulation performance for the PMSM drive system using different control schemes.

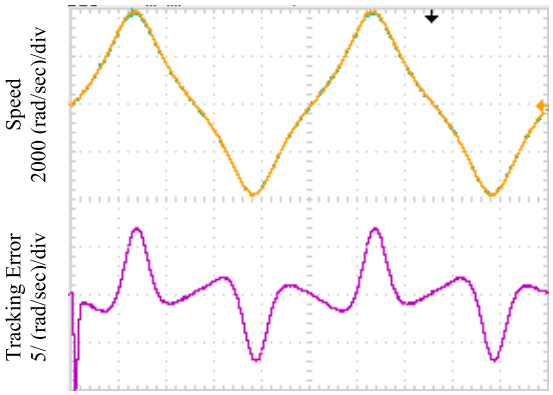

FIGURE 23. Experimental results of the PMSM using OAGSTSMC without external disturbance.

system to compare them with the proposed OAGSTSMC. The simulation results of the comparative PMSM dynamic response without any external disturbances are shown in Figs. (6)-(10). Fig. 6 depicts the PMSM dynamic response using the PID control scheme. The dynamic performance of the drive system using SMC scheme is introduced in Fig. 7. The PMSM dynamic response via employing the STSMC scheme for the similar operating conditions is given in Fig. 8. At the similar operating conditions, the dynamic response of the drive system using the ASTSMC approach is depicted in Fig. 9. The PMSM dynamic response via using the OAGSTSMC is depicted in Fig. 10. According to Fig. 10, the proposed OAGSTSMC converges quicker than other four controllers and tracks the target trajectory with minimum tracking errors. According to these results, the maximum tracking speed errors via the PID is nearly 6.966 rad/sec, the SMC is 6.376 rad/sec, the STSMC is 5.533 rad/sec, the ASTSMC is 2.731 rad/sec and the OAGSTSMC is 0.873 rad/sec. Therefore, the proposed OAGSTSMC compared with other controllers tracks the target trajectory with less tracking errors. As depicted in Fig. 11, the quicker convergence of tracking of the target trajectory through the longitudinal as well as transverse directions is similarly evident.

Similarly, the simulation results of the PMSM dynamic response by applying the external disturbance of 0.5 mN.m at t = 1.25 sec and removed at t = 3.75 sec and then repeated again are illustrated in Fig. 12 to Fig. 16. The drive system dynamic response from top to bottom are the speed command and actual rotor speed, tracking speed error and the *d-q* axis reference as well as actual currents in the rotating and stationary reference frames, respectively. Fig. 12 provides the PMSM dynamic response using the PID control approach. Fig. 13 illustrates the PMSM dynamic performance using SMC scheme. The dynamic response of the drive system via employing the STSMC scheme for the similar operating conditions is introduced in Fig. 14. At the similar operating conditions, the PMSM dynamic

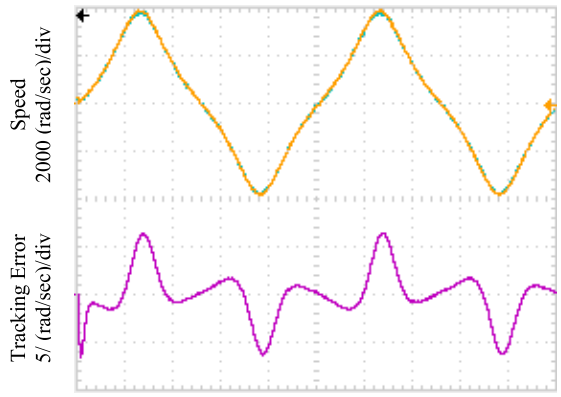

FIGURE 24. Experimental validation results of the PMSM using SMC without external disturbance.

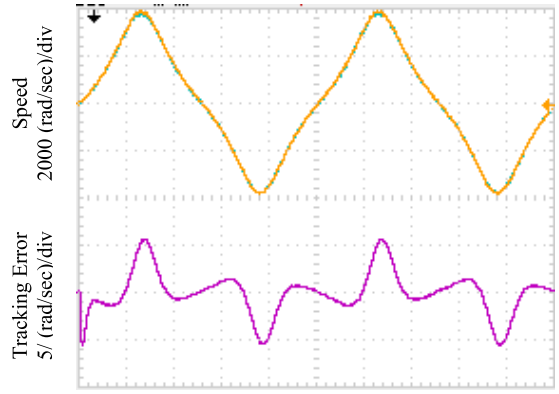

FIGURE 25. Experimental validation results of the PMSM using STSMC without external disturbance.

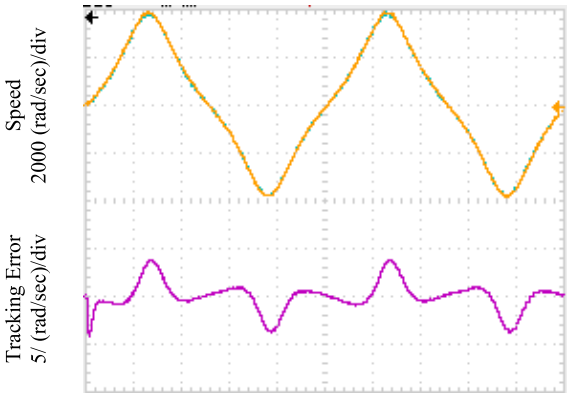

FIGURE 26. Experimental validation results of the PMSM using ASTSMC without external disturbance.

response using the ASTSMC scheme is depicted in Fig. 15. The dynamic response of the drive system via using the OAGSTSMC is given in Fig. 16. Additionally, the capabilities of external disturbance rejection are investigated as shown in Fig. 17 to Fig. 21. From the simulation results shown in Fig. 12 to Fig. 15 and Fig. 17 to Fig. 20, at the full load condition, the PID controller makes the rotor speed follow the desired speed with a maximum dip nearly 300 rad/sec

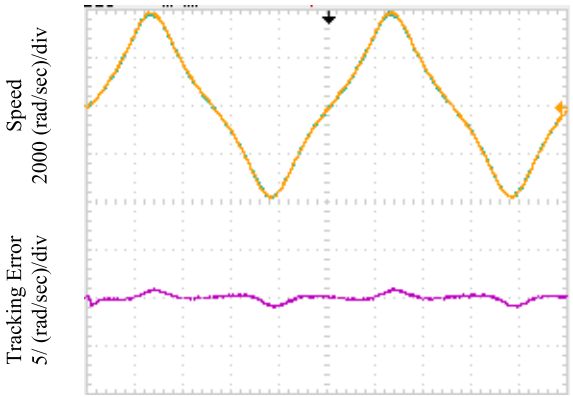

FIGURE 27. Experimental validation results of the PMSM using PID without external disturbance.

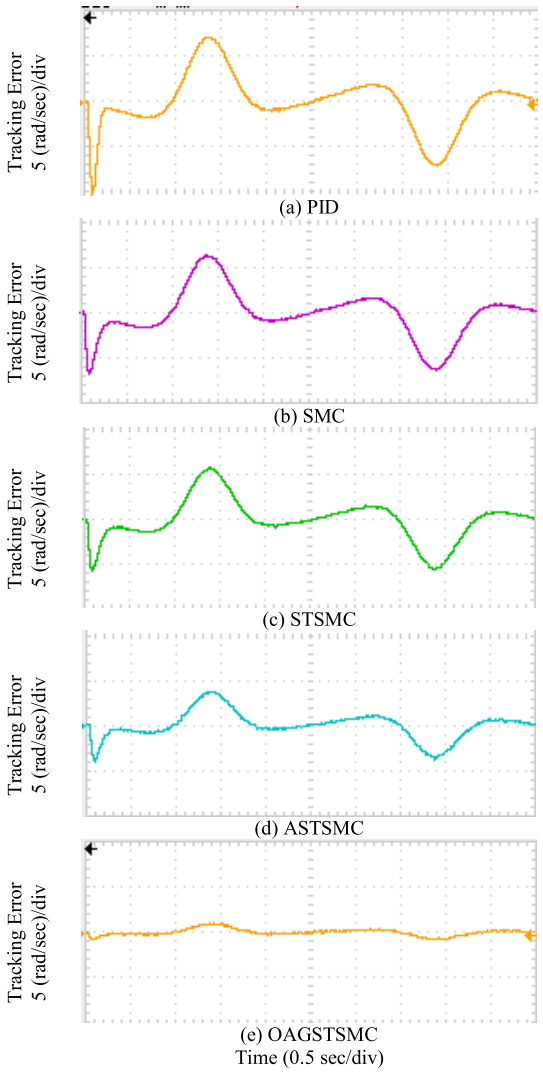

FIGURE 28. Enlarge experimental validation results of the rotor speed tracking error performance for the PMSM drive system using different control schemes.

(7.96%) with a recovery time nearly 0.5 sec. Utilizing the SMC, the maximum dip approached 140 rad/sec (3.71%) through a recovery time nearly 0.3 sec. Using STSMC

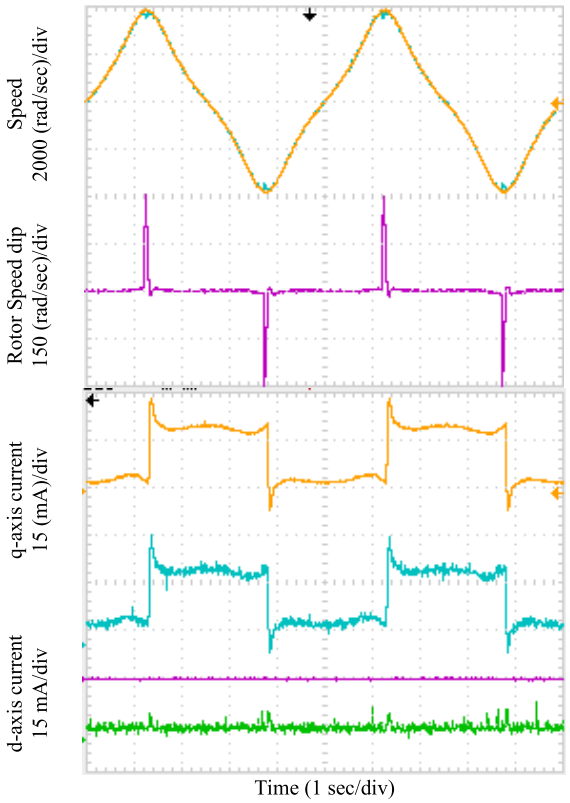

FIGURE 29. Experimental results of the PMSM dynamic performance using PID control scheme.

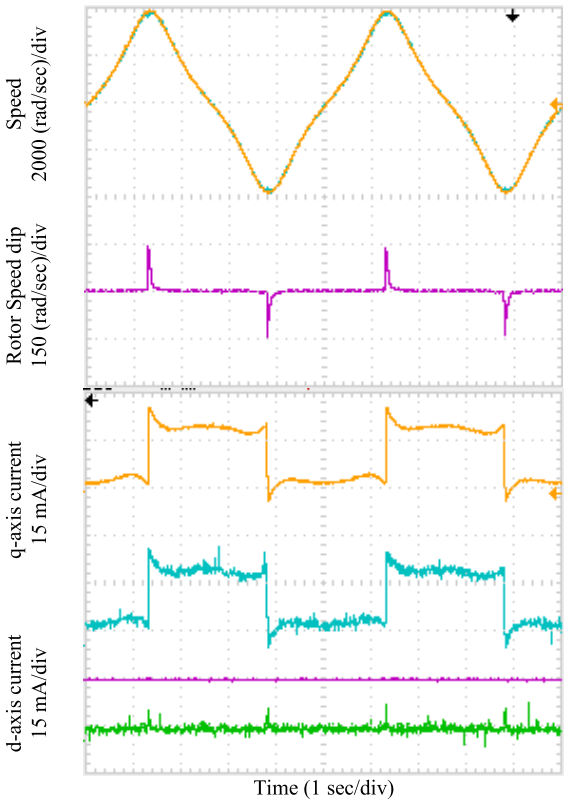

FIGURE 30. Experimental validation results of the PMSM dynamic performance using SMC control scheme.

the maximum dip reached to 74 rad/sec (1.96%) through a recovery time nearly 0.2 sec. Applying the ASTSMC, the maximum dip reached to 63 rad/sec (1.66%) through a recovery time nearly 0.15 sec. According to Fig. 16 and Fig. 21, which show the trajectory tracking of the drive system, the proposed OAGSTSMC converges quicker than other four controllers as well as follows the target trajectory with minimum tracking errors with a maximum dip nearly 30 rad/sec (0.79%) at full load within a recovery time of about 0.1 sec. The output signal of controller reveals the lowest level of overshoot compared with the other controllers. The comparison between the PID, SMC, STSMC, ASTSMC and OAGSTSMC control schemes during external disturbance regulation performance are given in Fig. 22. Obviously, the tracking errors rapidly approach zero that prove the OAGSTSMC approach robustness. Thus, the tracking errors have been minimized significantly and load regulation aptitudes have been investigated in comparison with the PID, SMC, STSMC along with ASTSMC control approaches. As a result, the designed OAGSTSMC structure has better control performance. Furthermore, the results have proved a significant minimization of the high dip of the PMSM rotor angular speed via employing the OAGSTSMC approach. Therefore, the proposed OAGSTSMC scheme performs better than PID, SMC, STSMC and ASTSMC control schemes in minimizing tracking errors, chattering level, as well as control effort. Eventually, the proposed OAGSTSMC approach provides numerous merits based on its robustness, tracking accuracy, optimality and suitability with the control of the PMSM.

D. EXPERIMENTAL VALIDATION RESULTS

The PMSM hardware laboratory setup with the same parameters used in the SIMULINK model is verified to investigate the developed OAGSTSMC compared to the PID, SMC, STSMC and ASTSMC approaches. The experimental tests are done based on the control approaches depicted in Fig. 1 through Fig. 5. The results of applying the proposed OAGSTSMC to the experimental setup of PMSM drive system shown in Fig. 5 are demonstrated. Indeed to OAGSTSMC, the PID, SMC, STSMC along with ASTSMC approaches are applied to the same system for conducting a comparative study. The desired speed trajectory is chosen as in simulation section. The experimental results of the comparative dynamic performance without external disturbance are shown in Fig. 23 to Fig. 27. Fig. 23 depicts the dynamic performances via employing the PID control, Fig. 24 depicts the performance of the SMC, Fig. 25 depicts the STSMC for the similar operating conditions, Fig. 26 shows the performance of the ASTSMC meanwhile Fig. 27 depicts the OAGSTSMC performance. From the trajectory tracking shown in Fig. 27, the OAGSTSMC converges quicker than PID, SMC, STSMC and ASTSMC as well as follows

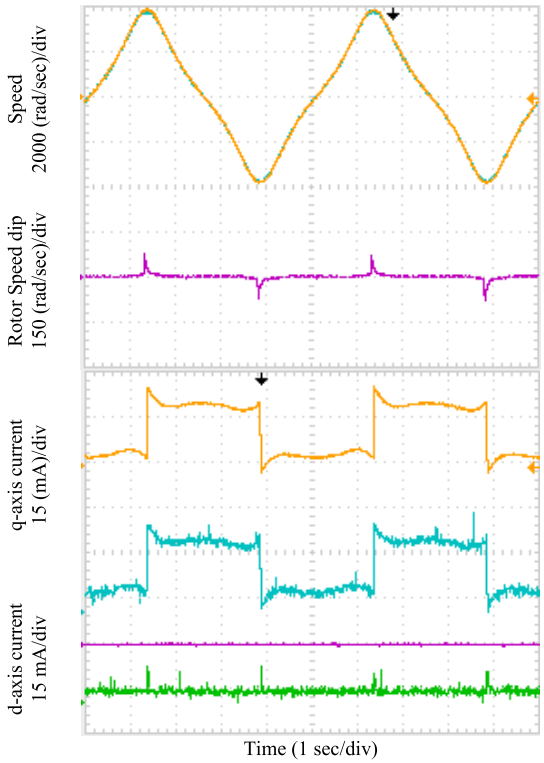

FIGURE 31. Experimental results of the PMSM drive dynamic performance using STSMC control scheme.

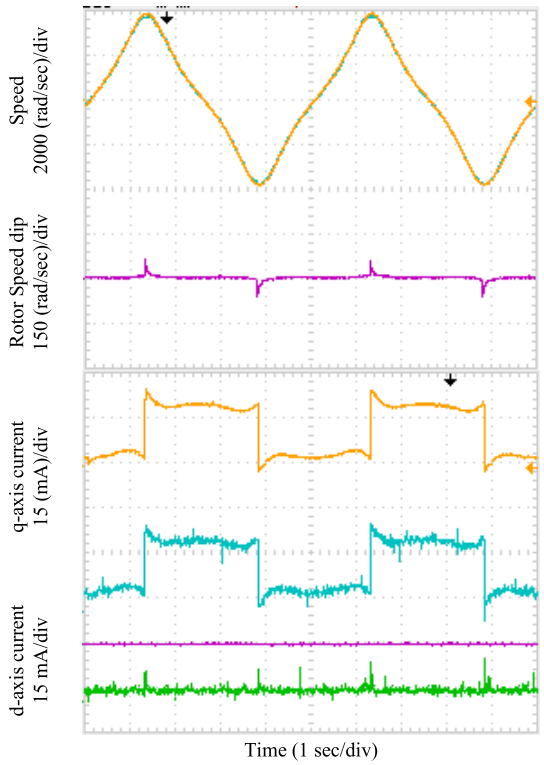

FIGURE 32. Experimental results of the PMSM drive dynamic performance using ASTSMC control scheme.

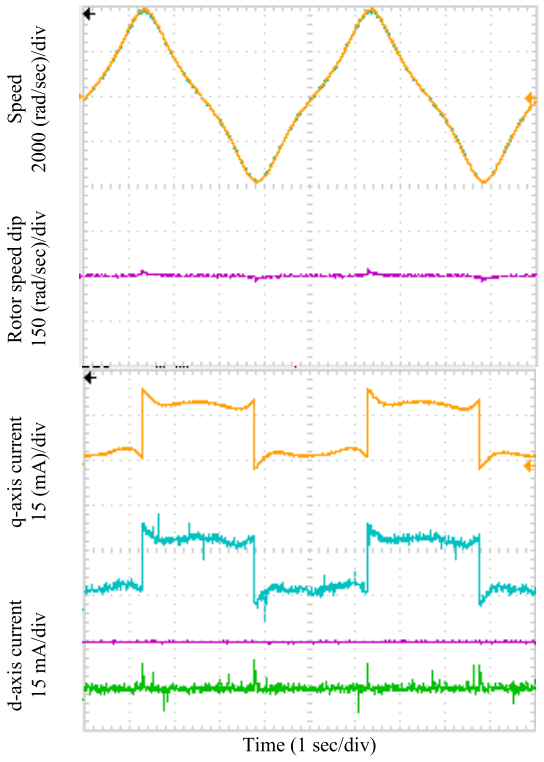

FIGURE 33. Experimental validation results of the PMSM dynamic performance using OAGSTSMC control scheme.

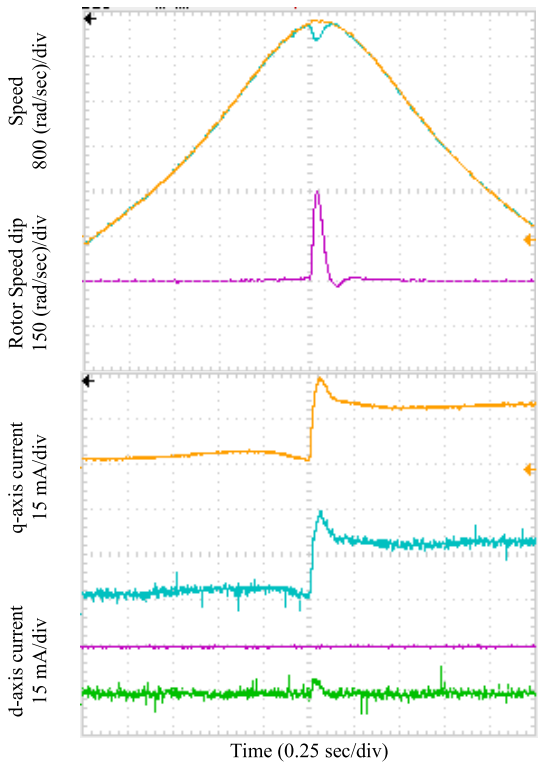

FIGURE 34. Enlarge experimental validation results of the load regulation performance for the PMSM drive using PIDC scheme.

the target trajectory with less tracking errors. From these results, it is obvious that the OAGSTSMC in comparison to the PID, SMC, STSMC and ASTSMC follows the desired trajectory accurately with robust performance as demonstrated in Fig. 28. Similarly, the experimental results by applying the external disturbance condition given in

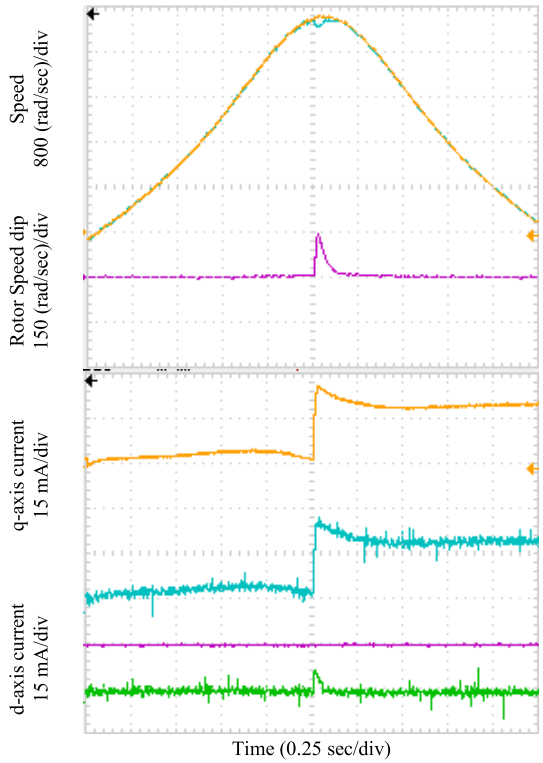

FIGURE 35. Enlarge experimental validation results of the load regulation performance for the PMSM drive via SMC scheme.

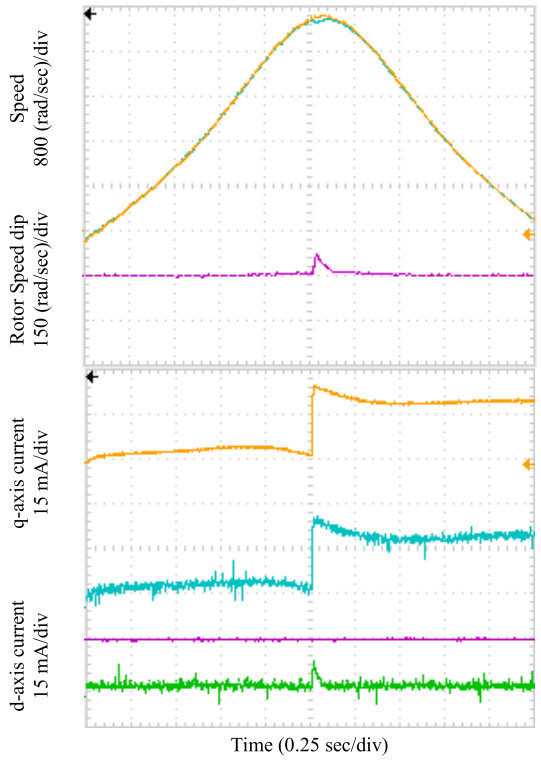

FIGURE 36. Enlarge experimental validation results of the load regulation performance for the PMSM drive via STSMC scheme.

simulation are illustrated in Fig. 29 to Fig. 33. The dynamic response from top to bottom are the speed command and actual rotor speed, tracking speed error and the *d-q* axis reference as well as actual currents in the rotating reference frame, respectively. The dynamic performances using the PID control is depicted in Fig. 29, the SMC is introduced in Fig. 30, the STSMC for the similar operating conditions is given in Fig. 31, the ASTSMC is given in Fig. 32 and the OAGSTSMC is given in Fig. 33. Enlarge dynamic response of external disturbance capabilities of the PID, SMC, STSMC, ASTSMC and OAGSTSMC are introduced in Fig. 34 to Fig. 38, respectively. From the trajectory tracking and load regulation performance shown in Fig. 33 and Fig. 38, obviously the OAGSTSMC converges quicker than PID, SMC, STSMC and ASTSMC as well as tracks the target trajectory in less tracking errors and less rotor speed dip at full load condition. The tracking errors rapidly approach zero that endorse the OAGSTSMC robustness. Thus, the tracking errors and the speed dip have been reduced significantly and the load regulation aptitudes have been confirmed versus the PID, SMC, STSMC and ASTSMC schemes. From these results, it is obvious that the OAGSTSMC follows the desired trajectory accurately with robust and optimal control performance for PMSM drive system. In addition, the control performances are continuously improved using the proposed OAGSTSMC despite PMSM drive is impacted by the external load torque disturbance as well as the disturbances from the unknown internal system dynamics and parameter uncertainties.

E. ASSESSMENT AND COMPARISON OF CONTROL RESPONSE

In this section, the results of applying OAGSTSMC to the PMSM are presented. To illustrate the advantages and effectiveness of the proposed OAGSTSMC, the PID, SMC, STSMC, and ASTSMC are also applied for comparison. For accurate evaluation for the proposed OAGSTSMC along with quantitative comparison of its response with other controllers, three response indices are taking into account namely maximum tracking error (MTE) average tracking errors (ATE), as well as standard deviation of tracking error (SDTE) [20]. The control performance can be readily compared via (69)-(71) as:

$$\text{MTE} = \max_k \sqrt{T(k)^2} \tag{69}$$

$$\text{ATE} = \sum_{k=1}^{n} \frac{T(k)}{n} \tag{70}$$

$$\text{SDTE} = \sqrt{\sum_{k=1}^{n} \frac{(T(k) - T_{mean})^2}{n}} \tag{71}$$

where. $T(k) = [\omega_r^m(k) - \omega_r(k)]$.

In Fig. 39, numerous comparative performance evaluations according to the MTE, ATE along with SDTE are introduced for OAGSTSMC, the PID, SMC, STSMC, and ASTSMC. For investigating the performance of these controllers, numerical results are performed via the performance indices that are illustrated in Table 3. These numerical results

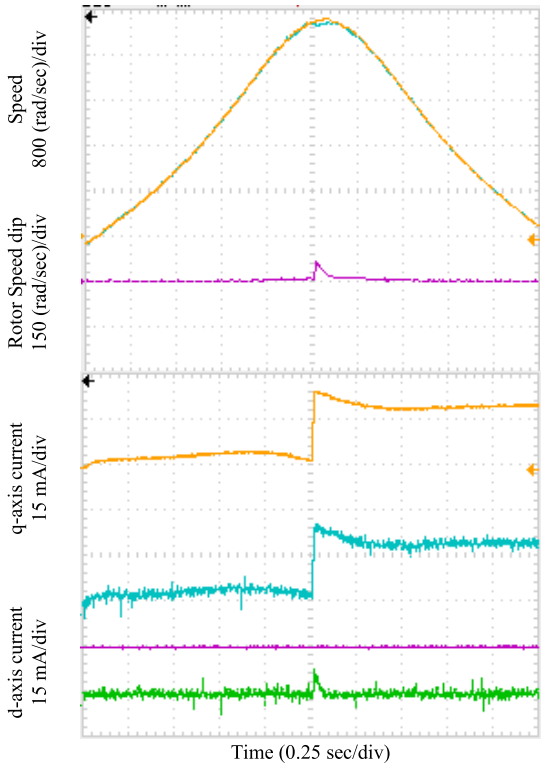

FIGURE 37. Enlarge experimental validation results of the load regulation performance for the PMSM drive via ASTSMC scheme.

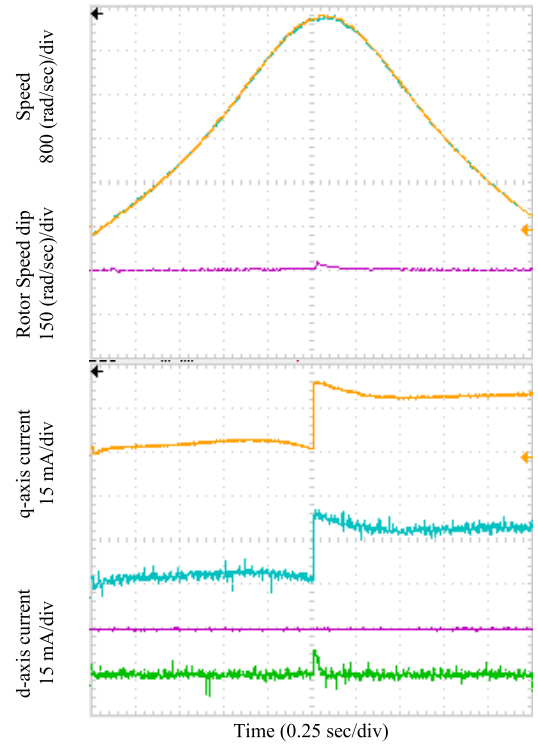

FIGURE 38. Enlarge experimental validation results of the load regulation performance for the PMSM drive via OAGSTSMC scheme.

illustrate the OAGSTSMC superiority compared with other four controllers. Entirely of the MTE, ATE along with SDTE indicators have smaller values for the OAGSTSMC than

TABLE 3. The PMSM performance evaluation.

Controller Type	Tracking Errors (rad/sec)		
	MTE	ATE	SDTE
PID	6.966	-0.0938	2.885
SMC	6.376	-0.0827	2.627
STSMC	5.533	-0.0769	2.280
ASTSMC	2.731	-0.0514	1.537
OAGSTSMC-	0.873	-0.0123	0.360

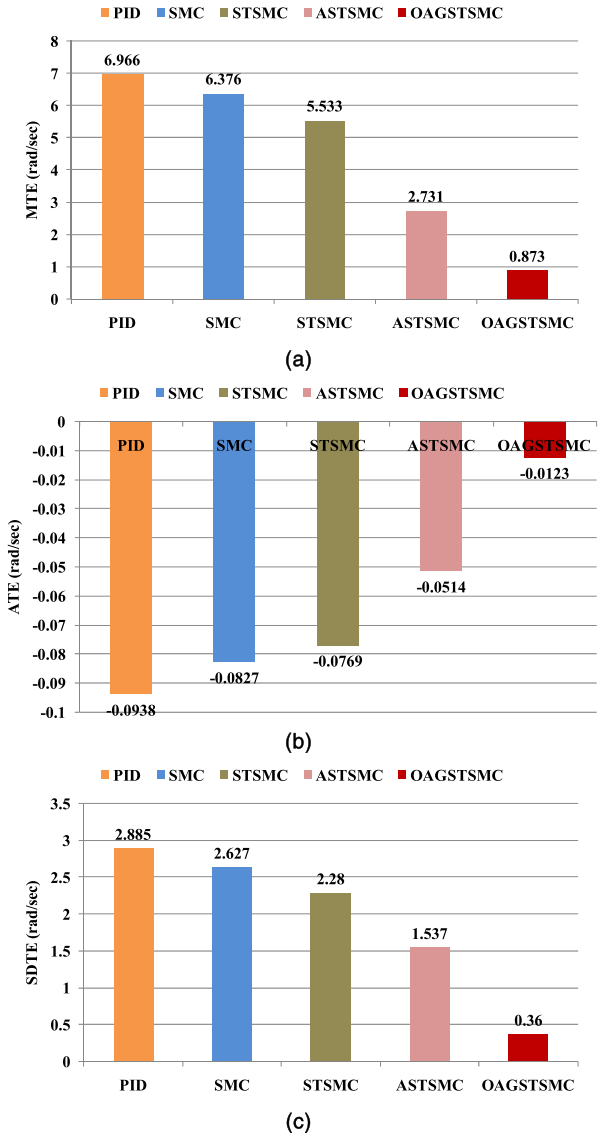

FIGURE 39. Performance evaluation of the PID, SMC, STSMC, ASTSMC and OAGSTSMC schemes for PMSM. (a) MTE, (b) ATE, along with (c) SDTE.

the PID, SMC, STSMC, and ASTSMC. This indicates the OAGSTSMC merits in more tracking precision. The results similarly indicate the STSMC and ASTSMC superiority versus the PID along with SMC for all of these indexes as given in Fig. 39. The regulation of external disturbance capabilities for the five controllers is given in Fig. 40. Fig. 40 depicts the maximum speed dip characteristics of the PID, SMC,

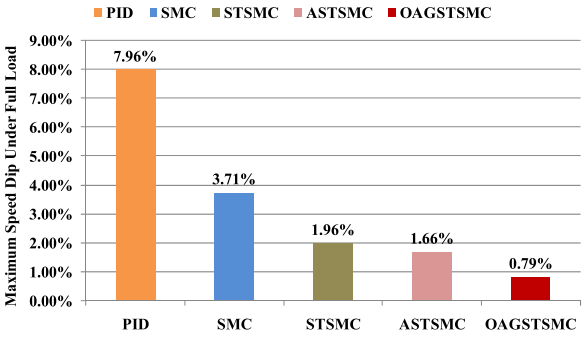

FIGURE 40. Maximum speed dip characteristics of the PID, SMC, STSMC, ASTSMC and OAGSTSMC schemes under full load condition for the PMSM drive system.

TABLE 4. Features of control schemes.

Control Scheme	PMSM Parameters	Robustness	Learning Ability	Computation Time
PID	Necessary	Fair	None	Low
SMC	Necessary	Fair	None	Low
STSMC	Necessary	Good	None	Medium
ASTSMC	Needless	Good	Online	> Medium
OAGSTSMC	Needless	Favorable	Online	> Medium

STSMC, ASTSMC and OAGSTSMC schemes under full load condition for the PMSM drive system. It is evident that the proposed OAGSTSMC has better external load disturbance regulation performance with decreased speed dip in comparison with PID, SMC, STSMC and ASTSMC schemes. Fig. 40 illustrates the tracking errors enhancement via the OAGSTSMC along with ASTSMC approaches compared with the PID, SMC and STSMC approaches. As depicted, the response measures of the PMSM are considerably improved via employing the proposed OAGSTSMC. Accordingly, the OAGSTSMC via actor-critic online algorithm achieve precise demands. Therefore, the proposed OAGSTSMC has proved its effectiveness for the PMSM drive system speed control for industrial applications in comparison with the other applied controllers.

Although the computation burden of the proposed OAGSTSMC is larger than the PID, SMC, STSMC and ASTSMC approaches to accomplish the control algorithms and adaptive laws, the superiority of control performance is achieved. Nowadays, high-performance DSPs are utilized to give flexible environments with high implementation rates for sophisticated control approaches. The features of different control schemes are summarized in Table 4.

VII. CONCLUSION

In this paper, a novel OAGSTSMC scheme utilizing actor-critic neural networks for applying on PMSM drive system with the target of increasing the tracking precision as well reducing the maximum speed dip under external disturbances has been presented. First, the SMC has been designed for stabilizing the PMSM. Afterwards, for improving the control system response, the STSMC has been adopted for reducing chattering. Nevertheless, the control performance can be destroyed due to external disturbances and unidentified internal system dynamics along with parameter uncertainties of the PMSM drive system. As well, the control performance may be affected due to the conservative selection of the STSMC gains. Therefore, an ASTSMC scheme is adopted to improve the control performance by avoiding the constraints on knowing the uncertainties along with disturbances upper bounds. Afterwards, for fulfilling the robustness, adaptive and optimal control performance of the drive PMSM system, the HDP is used for the optimal tuning of OAGSTSMC gains. Accordingly, an online actor-critic algorithm with HDP is designed for facilitating the online solution of the HJB equation via a critic neural network while seeking an optimal control via an actor neural network at the same time. Furthermore, via employing Lyapunov approach, the closed-loop control system stability is assured. The MATLAB/SIMULINK results along with the experimental validation results confirmed the OAGSTSMC superiority in minimizing the tracking errors, level of chattering as well as rotor speed dip at external load disturbance in comparison to PID, SMC, STSMC and ASTSMC schemes. The contributions of this paper are implementing along with developing a novel OAGSTSMC scheme to be applied on the PMSM drive to achieve adaptive, robust, and optimal control performance against significant disturbances.

APPENDIX

A. ON-LINE LEARNING ALGORITHMS USING GRADIENT-DESCENT TECHNIQUE

Fig. 2 depicts the online learning of the control algorithms for approximating the HJB equation via the critic neural network though pursuing an optimal control via actor neural network at the same time. The gradient descent algorithm for computing the actor as well critic neural networks the optimal weights is suggested for implementing the online direct HDP controller [73], [75].

1) THE CRITIC NEURAL NETWORK ONLINE LEARNING ALGORITHMS

The gradient-descent adaptation algorithm is employed for updating the weights of the critic NN. Updating laws of $\varpi_{c1,ij}(t)$ & $\varpi_{c2,ij}(t)$ can be expressed as:

$$\begin{aligned}\Delta\varpi_{c2,j}(t) &= -\eta_c(t)\frac{\partial E_c}{\partial \varpi_{c2,j}} = -\eta_c(t)\frac{\partial E_c}{\partial \hat{J}(t)}\frac{\partial \hat{J}(t)}{\partial \varpi_{c2,j}} \\ &= -\eta_c(t)\beta e_c(t)\Theta_{cj}(t) \qquad \text{(A1)}\\ \Delta\varpi_{c1,ij}(t) &= -\eta_c(t)\frac{\partial E_c(t)}{\partial \varpi_{c1,ij}(t)} \\ &= -\eta_c(t)\frac{\partial E_c(t)}{\partial \hat{J}(t)}\frac{\partial \hat{J}(t)}{\partial \Theta_{cj}(t)}\frac{\partial \Theta_{cj}(t)}{\partial \Phi_{cj}(t)}\frac{\partial \Phi_{cj}(t)}{\partial \varpi_{c1,ij}(t)} \\ &= -\eta_c(t)\beta e_c(t)\varpi_{c2,j}(t)[(1-\Theta_{cj}^2(t))/2]z_i(t) \qquad \text{(A2)}\end{aligned}$$

The weights can be updated via employing (A3) & (A4):

$$\varpi_{c2,j}(t+\Delta t)=\varpi_{c2,j}(t)+\Delta\varpi_{c2,j}(t) \tag{A3}$$
$$\varpi_{c1,ij}(t+\Delta t)=\varpi_{c1,ij}(t)+\Delta\varpi_{c1,ij}(t) \tag{A4}$$

where $\eta_c(t)>0$ denotes the critic neural network learning rate parameter of the connecting weights within instant t that regularly decays with time to an insignificant value. $\varpi_{c1,ij}(t)$ & $\varpi_{c2,ij}(t)$ are the weight vectors within the critic network.

2) THE ACTOR NEURAL NETWORK ONLINE LEARNING ALGORITHMS

Likewise, the gradient-descent adaptation algorithm is used for the weights updating of the actor neural network. Updating laws of $\varpi_{a1,ij}(t)$ and $\varpi_{a2,jk}(t)$ are given by:

$$\begin{aligned}
&\Delta\varpi_{a2,jk}(t)\\
&=-\eta_a(t)\frac{\partial E_a}{\partial\varpi_{a2,jk}(t)}\\
&=-\eta_a(t)\frac{\partial E_a}{\partial\hat{J}(t)}\frac{\partial\hat{J}(t)}{\partial\Xi_{ack}(t)}\frac{\partial\Xi_{ack}(t)}{\partial\Omega_{ak}(t)}\frac{\partial\Omega_{ak}(t)}{\partial\varpi_{a2,jk}(t)}\\
&=-\eta_a(t)e_a(t)\varpi_{c2,j}(t)[(1-\Xi_{ack}^2(t))/2]\Theta_{aj}(t)\\
&\quad\cdot\sum_{i=1}^{N_{ch}}\left[\varpi_{a2,jk}(t)[(1-\Theta_{cj}^2(t))/2]\varpi_{a1,ij}(t)\right]
\end{aligned}\tag{A5}$$

$$\begin{aligned}
&\Delta\varpi_{a1,ij}(t)\\
&=-\eta_a(t)\frac{\partial E_a}{\partial\varpi_{a1,ij}(t)}\\
&=-\eta_a(t)\frac{\partial E_a}{\partial\hat{J}(t)}\frac{\partial\hat{J}(t)}{\partial\Xi_{ack}(t)}\frac{\partial\Xi_{ack}(t)}{\partial\Omega_{ak}(t)}\frac{\partial\Omega_{ak}(t)}{\partial\Theta_{aj}(t)}\\
&\quad\cdot\frac{\partial\Theta_{aj}(t)}{\partial\Phi_{aj}(t)}\frac{\partial\Phi_{aj}(t)}{\partial\varpi_{a1,ij}(t)}\\
&=-\eta_a(t)e_a(t)[(1-\Xi_{ack}^2(t))/2]\varpi_{c2,j}(t)[(1-\Theta_{cj}^2(t))/2]z_i\\
&\quad\cdot\sum_{i=1}^{N_{ch}}\left[\varpi_{a2,jk}(t)[(1-\Theta_{cj}^2(t))/2]\varpi_{a1,ij}(t)\right]
\end{aligned}\tag{A6}$$

The weights are updated using (A7) and (A8):

$$\varpi_{a2,jk}(t+\Delta t)=\varpi_{a2,jk}(t)+\Delta\varpi_{a2,jk}(t) \tag{A7}$$
$$\varpi_{a1,ij}(t+\Delta t)=\varpi_{a1,ij}(t)+\Delta\varpi_{a1,ij}(t) \tag{A8}$$

where $\eta_a(t)>0$ denotes the actor neural network learning rate parameter of the connecting weights at instant t that is regularly decays with time to a small value. $\varpi_{a1,ij}(t)$ &$\varpi_{a2,jk}(t)$ are the weight vectors within the actor network.

B. STABILITY ANALYSIS

The Lyapunov stability framework in the following section, is adopted for proving the UUB property of (66) and (67).

1) LEMMA 1

Consider the output of the critic neural network is given as (59), the critic neural network weights update according to (61) and Assumption 1 is fulfilled, afterwards for

$$V_1(t)=\frac{1}{\eta_c}\mathrm{tr}[\tilde{W}_c^T(t)\tilde{W}_c(t)] \tag{A9}$$

The 1st difference of $V_1(t)$ is expressed by (A10).

$$\begin{aligned}
&\Delta V_1(t)\\
&\le-\beta^2\left\|\varepsilon_c(t)\right\|^2-\beta^2(1-\eta_c\beta^2\left\|\Theta_c(t)\right\|^2)\\
&\quad\times\Big\|\varepsilon_c(t)+W_c^T(t)\Theta_c(t)+\beta^{-1}r(t)\\
&\quad-\beta^{-1}\hat{W}_c^T(t-\Delta t)\Theta_c(t-\Delta t)\Big\|^2\\
&\quad+2\left\|\beta W_c^T(t)\Theta_c(t)+r(t)-\frac{1}{2}\hat{W}_c^T(t-\Delta t)\Theta_c(t-\Delta t)\right.\\
&\quad\left.-\frac{1}{2}W_c^T(t)\Theta_c(t-\Delta t)\right\|^2+\frac{1}{2}\left\|\varepsilon_c(t-\Delta t)\right\|^2
\end{aligned}\tag{A10}$$

where $\tilde{W}_c(t)=(\hat{W}_c(t)-W_c^*)$ represents the error between the optimal weights W_c^* along with its estimates $\hat{W}_c(t)$:

$$\varepsilon_c(t)=\left(\hat{W}_c(t)-W_c^*\right)^T\Theta_c(t)=\tilde{W}_c(t)\Theta_c(t) \tag{A11}$$

where $\varepsilon_c(t)$ represents the approximation error of the output of the critic neural network.

Proof of Lemma 1: The 1st difference of Lyapunov function candidate $V_1(t)$ can be expressed as:

$$\Delta V_1(t)=\frac{1}{\eta_c}\mathrm{tr}[\tilde{W}_c^T(t+\Delta t)\tilde{W}_c(t+\Delta t)-\tilde{W}_c^T(t)\tilde{W}_c(t)] \tag{A12}$$

Using the update law (61), the weight estimation error of the critic neural network can be expressed by (A13):

$$\begin{aligned}
\tilde{W}_c(t+\Delta t)&=\hat{W}_c(t+\Delta t)-W_c^*\\
&=\tilde{W}_c(t)-\eta_c(t)\beta\Theta_c(t)\\
&\quad\times\Big[\beta\hat{W}_c^T(t)\,\Theta_c(t)+r(t)-\hat{W}_c\\
&\quad\times(t-\Delta t)\Theta_c(t-\Delta t)\Big]^T
\end{aligned}\tag{A13}$$

The (A13) can be substituted into (A12), thus, (A14) can be obtained:

$$\begin{aligned}
\Delta V_1(t)=&-\beta^2\left\|\varepsilon_c(t)\right\|^2-\beta^2(1-\eta_c\beta^2\left\|\Theta_c(t)\right\|^2)\\
&\times\Big\|\varepsilon_c(t)+W_c^T(t)\Theta_c(t)+\beta^{-1}r(t)\\
&-\beta^{-1}\hat{W}_c^T(t-\Delta t)\Theta_c(t-\Delta t)\Big\|^2\\
&+\left\|\beta W_c^T(t)\Theta_c(t)+r(t)-\hat{W}_c^T(t-\Delta t)\Theta_c(t-\Delta t)\right\|^2
\end{aligned}\tag{A14}$$

Using the Cauchy-Schwarz inequality, (A10) can be obtained [73], [75].

2) LEMMA 2

Consider the actor neural network output is given by (60), the actor neural network weights update according to (62) and Assumption 1 is fulfilled, afterwards for

$$V_2(t) = \frac{1}{\varsigma\eta_a}\text{tr}\left[\tilde{W}_a^T(t)\tilde{W}_a(t)\right] \tag{A15}$$

The 1st difference of $V_2(t)$ can be expressed by (A16):

$$\begin{aligned}
&\Delta V_2(t)\\
&\le \frac{1}{\varsigma}\left\{-\left[\left\|\hat{W}_c^T(t)G(t)\right\|^2 - \eta_a(t)\left\|\hat{W}_c^T(t)G(t)\right\|^2\|\Theta_a(t)\|^2\right]\right.\\
&\quad\times\left\|W_c^T(t)\Theta_c(t)\right\|^2 + \left\|\hat{W}_c^T(t)G(t)\right\|^2\|\varepsilon_a(t)\|^2\\
&\quad\left.+4\left\|W_c^T(t)\Theta_c(t)\right\|^2 + 4\|\varepsilon_c(t)\|^2\right\}
\end{aligned} \tag{A16}$$

where $\tilde{W}_a(t) = (\hat{W}_a(t) - W_a^*)$ represents the error difference between the optimal weights W_a^* and its estimates $\hat{W}_a(t)$:

$$\varepsilon_a(t) = \left(\hat{W}_a(t) - W_a^*\right)^T\Theta_a(t) = \tilde{W}_a(t)\Theta_a(t) \tag{A17}$$

where $\varepsilon_a(t)$ denotes the approximation error of the output of the actor neural network as well as $\varsigma > 0$ denotes the weighting factor.

Lemma 2 Proof: The 1st difference of Lyapunov function candidate $V_2(t)$ is expressed as in (A18):

$$\Delta V_2(t) = \frac{1}{\varsigma\eta_c}\text{tr}\left[\tilde{W}_a^T(t+\Delta t)\tilde{W}_a(t+\Delta t) - \tilde{W}_a^T(t)\tilde{W}_a(t)\right] \tag{A18}$$

Using the update law (62), the weight estimation error of the actor neural network is given by:

$$\begin{aligned}
&\tilde{W}_a(t+\Delta t)\\
&= \hat{W}_a(t+\Delta t) - W_a^*\\
&= \tilde{W}_a(t) - \eta_a(t)\,\Theta_a(t)[\hat{W}_c^T(t)G(t)][\hat{W}_c^T(t)\Theta_c(t)]^T
\end{aligned} \tag{A19}$$

Substituting (A19) into (A18) one gets:

$$\begin{aligned}
&\Delta V_2(t)\\
&= \frac{1}{\varsigma}\left\{-2[\hat{W}_c^T(t)G(t)]\varepsilon_a(t)\left(\hat{W}_c^T(t)\Theta_c(t)\right)^T\right.\\
&\quad\left.+\eta_a(t)\left\|\hat{W}_c^T(t)G(t)\right\|^2\|\Theta_a(t)\|^2\left\|W_c^T(t)\Theta_c(t)\right\|^2\right\}
\end{aligned} \tag{A20}$$

The 1st difference of $V_2(t)$ is expressed by (A21):

$$\begin{aligned}
&\Delta V_2(t)\\
&= \frac{1}{\varsigma}\left\{-\left[\left\|\hat{W}_c^T(t)G(t)\right\|^2 - \eta_a(t)\left\|\hat{W}_c^T(t)G(t)\right\|^2\|\Theta_a(t)\|^2\right]\right.\\
&\quad\times\left\|W_c^T(t)\Theta_c(t)\right\|^2 - \left\|\hat{W}_c^T(t)G(t)\right\|^2\|\varepsilon_a(t)\|^2\\
&\quad\left.+\left\|W_c^T(t)\Theta_c(t) - \hat{W}_c^T(t)G(t)\varepsilon_a(t)\right\|^2\right\}
\end{aligned} \tag{A21}$$

Using the Cauchy-Schwarz inequality, (A16) can be obtained [73], [75], [76].

3) PROOF OF THEOREM 2

Select a Lyapunov function candidate to be (A22):

$$\begin{aligned}
V_t(t) &= V_1(t) + V_2(t) + V_3(t)\\
&= \frac{1}{\eta_c}\text{tr}[\tilde{W}_c^T(t)\tilde{W}_c(t)] + \frac{1}{\varsigma\eta_a}\text{tr}\left[\tilde{W}_a^T(t)\tilde{W}_a(t)\right]\\
&\quad+\frac{1}{2}\|\varepsilon_c(t-\Delta t)\|^2
\end{aligned} \tag{A22}$$

where $\varsigma > 0$ denotes the weighting factor.

The 1st difference of $V(t)$ is expressed by (A23).

$$\Delta V(t) = V(t+\Delta t) - V(t) = \Delta V_1(t) + \Delta V_2(t) + \Delta V_3(t) \tag{A23}$$

$$V_3(t) = \frac{1}{2}\|\varepsilon_c(t-\Delta t)\|^2 \tag{A24}$$

The first difference of $V_3(t)$ is expressed by (A25).

$$\Delta V_3(t) = \frac{1}{2}\left[\|\varepsilon_c(t)\|^2 - \|\varepsilon_c(t-\Delta t)\|^2\right] \tag{A25}$$

Substituting the results of Lemma 1 (A10), Lemma 2 (A16) in (A23) and using Assumption 1, the following result is obtained:

$$\begin{aligned}
&\Delta V_1(t)\\
&= \Delta V_1(t) + \Delta V_2(t) + \Delta V_3(t)\\
&\le -\left(\beta^2 - \frac{1}{2} - \frac{4}{\varsigma}\right)\|\varepsilon_c(t)\|^2 - \beta^2(1 - \eta_c\beta^2\|\Theta_c(t)\|^2)\\
&\quad\times\left\|\varepsilon_c(t) + W_c^T(t)\Theta_c(t) + \beta^{-1}r(t)\right.\\
&\quad\left.-\beta^{-1}\hat{W}_c^T(t-\Delta t)\Theta_c(t-\Delta t)\right\|^2\\
&\quad-\left[\left\|\hat{W}_c^T(t)G(t)\right\|^2 - \eta_a(t)\left\|\hat{W}_c^T(t)G(t)\right\|^2\|\Theta_a(t)\|^2\right]\\
&\quad\times\left\|W_c^T(t)\Theta_c(t)\right\|^2 + 2\left\|\beta W_c^T(t)\Theta_c(t) + r(t)\right.\\
&\quad\left.-\frac{1}{2}\hat{W}_c^T(t-\Delta t)\Theta_c(t-\Delta t) - \frac{1}{2}W_c^T(t)\Theta_c(t-\Delta t)\right\|^2\\
&\quad+\frac{1}{\varsigma}\left\|\hat{W}_c^T(t)G(t)\right\|^2\|\varepsilon_a(t)\|^2 + \frac{4}{\varsigma}\left\|W_c^T(t)\Theta_c(t)\right\|^2
\end{aligned} \tag{A26}$$

Using the conditions in (68) and choose ς to satisfy the following condition:

$$\varsigma > \frac{4}{\left(\beta^2 - 1/2\right)} \tag{A27}$$

The first difference (A26) can be expressed as:

$$\begin{aligned}
&\Delta V_1(t)\\
&= \Delta V_1(t) + \Delta V_2(t) + \Delta V_3(t)\\
&\le -\left(\beta^2 - \frac{1}{2} - \frac{4}{\varsigma}\right)\|\varepsilon_c(t)\|^2 - \beta^2(1 - \eta_c\beta^2\|\Theta_c(t)\|^2)\\
&\quad\times\left\|\varepsilon_c(t) + W_c^T(t)\Theta_c(t) + \beta^{-1}r(t)\right.\\
&\quad\left.-\beta^{-1}\hat{W}_c^T(t-\Delta t)\Theta_c(t-\Delta t)\right\|^2
\end{aligned}$$

$$-\frac{1}{\varsigma}\left[\left\|\hat{W}_c^T(t)G(t)\right\|^2-\eta_a(t)\left\|\hat{W}_c^T(t)G(t)\right\|^2\|\Theta_a(t)\|^2\right]\times\left\|W_c^T(t)\Theta_c(t)\right\|^2+\aleph^2 \tag{A28}$$

where $\aleph^2$ is given by

$$\aleph^2=2\left\|\beta W_c^T(t)\Theta_c(t)+r(t)-\frac{1}{2}\hat{W}_c^T(t-\Delta t)\Theta_c(t-\Delta t)-\frac{1}{2}W_c^T(t)\Theta_c(t-\Delta t)\right\|^2+\frac{1}{\varsigma}\left\|\hat{W}_c^T(t)G(t)\right\|^2\|\varepsilon_a(t)\|^2+\frac{4}{\varsigma}\left\|W_c^T(t)\Theta_c(t)\right\|^2 \tag{A29}$$

Using the Cauchy-Schwarz inequality, (A29) can be rewritten as:

$$\begin{aligned}\aleph^2&\le 8\left[\left\|W_c^T(t)\Theta_c(t)\right\|^2+r^2(t)\frac{1}{4}\left\|\hat{W}_c^T(t-\Delta t)\Theta_c(t-\Delta t)\right\|^2+\frac{1}{4}\left\|W_c^T(t)\Theta_c(t-\Delta t)\right\|^2\right]+\frac{2}{\varsigma}\left\|\hat{W}_c^T(t)G(t)\right\|^2\\&\times\left[\left\|W_a^T(t)\Theta_a(t)\right\|^2+\left\|W_a^T(t)\Theta_a(t)\right\|^2\right]+\frac{4}{\varsigma}\left\|W_c^T(t)\Theta_c(t)\right\|^2\\&\le\left(8\beta^2+4+\frac{4}{\varsigma}\right)W_{cM}^2\Theta_{cM}^2+\frac{4}{\varsigma}W_{cM}^2G_M^2W_{aM}^2\Theta_{aM}^2+8r_M^2=\aleph_M^2\end{aligned} \tag{A30}$$

where W_{cM}, W_{aM}, Θ_{cM}, Θ_{aM}, G_M along with r_M denote the upper bounds of $W_{cM}(t)$, $W_{aM}(t)$, $\Theta_{cM}(t)$, $\Theta_{aM}(t)$, $G_M(t)$ and $r_M(t)$, respectively.

If the conditions in (68) are fulfilled, afterwards for any:

$$\|\varepsilon_c(t)\|>\frac{\aleph_M}{\left(\beta^2-\frac{1}{2}-\frac{4}{\varsigma}\right)} \tag{A31}$$

The 1st difference $\Delta V(t)\le 0$ holds. Based on Lyapunov extension theorem [67], this proves that the errors between the optimal weights $W_a^*\&W_c^*$ along with their estimates $\hat{W}_a(t)$ & $\hat{W}_c(t)$are UUB, respectively.

REFERENCES

[1] K. Hameyer and R. Belmans, "Design of very small electromagnetic and electrostatic micro motors," *IEEE Trans. Energy Convers.*, vol. 14, no. 4, pp. 1241–1246, Dec. 1999.
[2] P. L. Chapman and P. T. Krein, "Smaller is better? [micromotors and electric drives]," *IEEE Ind. Appl. Mag.*, vol. 9, no. 1, pp. 62–67, Jan. 2003.
[3] D. P. Arnold and N. Wang, "Permanent magnets for MEMS," *J. Microelectromech. Syst.*, vol. 18, no. 6, pp. 1255–1266, Dec. 2009.
[4] H. Ishihara, F. Arai, and T. Fukuda, "Micro mechatronics and micro actuators," *IEEE/ASME Trans. Mechatronics*, vol. 1, no. 1, pp. 68–79, Mar. 1996.
[5] T. C. Neugebauer, D. J. Perreault, J. H. Lang, and C. Livermore, "A six-phase multilevel inverter for MEMS electrostatic induction micromotors," *IEEE Trans. Circuits Syst. II, Exp. Briefs*, vol. 51, no. 2, pp. 49–56, Feb. 2004.
[6] J. Zhang and M. Schroff, "High-performance micromotor control systems," in *Proc. 29th Annu. Conf. IEEE Ind. Electron. Soc. (IECON)*, Nov. 2003, pp. 347–352.
[7] J. Zhang and Q. Jiang, "Sensorless commutation of micro PMSMs for high-performance high-speed applications," in *Proc. Int. Conf. Electr. Mach. Syst.*, 2005, pp. 1795–1800.
[8] Y.-H. Chang, C.-C. Wu, and T.-H. Liu, "Design and implementation of an H_∞ controller for a micropermanent magnet synchronous motor position control system," *IET Electr. Power Appl.*, vol. 2, no. 1, pp. 8–18, Jan. 2008.
[9] Y.-H. Chang, T.-H. Liu, and C.-C. Wu, "Novel adjustable micropermanent-magnet synchronous motor control system without using a rotor-position/speed sensor," *IEE Proc.-Electr. Power Appl.*, vol. 153, no. 3, pp. 429–438, 2006.
[10] Y.-H. Chang, T.-H. Liu, and D.-F. Chen, "Design and implementation of a robust controller for a micro permanent magnet synchronous speed control systems," in *Proc. 2nd Int. Conf. Innov. Comput., Informatio Control (ICICIC)*, Sep. 2007, p. 99.
[11] S. E. Lyshevski, "Mini- and microscale closed-loop servodrives with brushless minimotors and ICs monolithic amplifiers/controllers," in *Proc. 41st IEEE Conf. Decis. Control*, Dec. 2002, pp. 3670–3674.
[12] A. Purushotham, S. L. Garverick, C. Edwards, and M. L. Nagy, "A closed-loop micromotor control system," in *Proc. IEEE Int. Symp. Circuits Syst. Circuits Syst. Connecting World (ISCAS)*, vol. 4, 1996, pp. 209–212, doi: 10.1109/ISCAS.1996.541937.
[13] F. F. M. El-Sousy and S. A. Al-Kharj, "Intelligent hybrid controller for identification and control of micro permanent-magnet synchronous motor servo drive system using Petri recurrent-fuzzy-neural-network," *WSEAS Trans. Syst. Control*, vol. 9, pp. 336–355, Jul. 2014.
[14] Y. H. Chang, T. H. Liu, and D. F. Chen, "Design and implementation of an adaptive inverse controller for a micro-permanent magnet synchronous control system," *IET. Electr. Power Appl.*, vol. 3, no. 5, pp. 471–481, 2009.
[15] T.-Y. Chou, T.-H. Liu, and T.-T. Cheng, "Sensorless micro-permanent magnet synchronous motor control system with a wide adjustable speed range," *IET Electr. Power Appl.*, vol. 6, no. 2, pp. 62–72, 2012.
[16] T. Y. Chou and T. H. Liu, "Implementation of a motion control system using micro-permanent magnet synchronous motors," *IET Electr. Power Appl.*, vol. 6, no. 6, pp. 362–374, Jul. 2012.
[17] W.-C. Chi and M.-Y. Cheng, "Implementation of a sliding-mode-based position sensorless drive for high-speed micro permanent-magnet synchronous motors," *ISA Trans.*, vol. 53, no. 2, pp. 444–453, Mar. 2014.
[18] F. F. M. El-Sousy and K. A. Abuhasel, "Nonlinear adaptive backstepping control-based dynamic recurrent RBFN uncertainty observer for high-speed micro permanent-magnet synchronous motor drive system," in *Proc. IEEE Energy Convers. Congr. Expo. (ECCE)*, Portland, OR, USA, Sep. 2018, pp. 1696–1703.
[19] F. F. M. El-Sousy, M. F. El-Naggar, M. Amin, A. Abu-Siada, and K. A. Abuhasel, "Robust adaptive neural-network backstepping control design for high-speed permanent-magnet synchronous motor drives: Theory and experiments," *IEEE Access*, vol. 7, pp. 99327–99348, 2019.
[20] F. F. M. El-Sousy, M. M. Amin, and O. A. Mohammed, "Robust optimal control of high-speed permanent-magnet synchronous motor drives via self-constructing fuzzy wavelet neural network," *IEEE Trans. Ind. Appl.*, vol. 57, no. 1, pp. 999–1013, Jan. 2021.
[21] F. F. M. El-Sousy, "Adaptive dynamic sliding-mode control system using recurrent RBFN for high-performance induction motor servo drive," *IEEE Trans. Ind. Informat.*, vol. 9, no. 4, pp. 1922–1936, Nov. 2013.
[22] S.-Y. Chen, H.-H. Chiang, T.-S. Liu, and C.-H. Chang, "Precision motion control of permanent magnet linear synchronous motors using adaptive fuzzy fractional-order sliding-mode control," *IEEE/ASME Trans. Mechatronics*, vol. 24, no. 2, pp. 741–752, Apr. 2019.
[23] L. Ma, H. Sun, and J. Song, "Fractional-order adaptive integral hierarchical sliding mode control method for high-speed linear motion of spherical robot," *IEEE Access*, vol. 8, pp. 66243–66256, 2020.
[24] J. Shi and Q. Zhang, "Dynamic sliding-mode control for T-S fuzzy singular time-delay systems with H_∞ performance," *IEEE Access*, vol. 7, pp. 115388–115399, 2019.
[25] S. Hou, J. Fei, Y. Chu, and C. Chen, "Experimental investigation of adaptive fuzzy global sliding mode control of single-phase shunt active power filters," *IEEE Access*, vol. 7, pp. 64442–64449, 2019.
[26] V. I. Utkin, "Sliding mode control design principles and applications to electric drives," *IEEE Trans. Ind. Electron.*, vol. 40, no. 1, pp. 23–36, Feb. 1993.
[27] V. I. Utkin, *Sliding Modes in Control and Optimization*. Berlin, Germany: Springer-Verlag, 1992.
[28] X. Yu and O. Kaynak, "Sliding-mode control with soft computing: A survey," *IEEE Trans. Ind. Electron.*, vol. 56, no. 9, pp. 3275–3285, Sep. 2009.

[29] L. Wang, J. Mishra, Y. Zhu, and X. Yu, "An improved sliding-mode current control of induction machine in presence of voltage constraints," *IEEE Trans. Ind. Informat.*, vol. 16, no. 2, pp. 1182–1191, Feb. 2020.

[30] L. Gou, C. Wang, M. Zhou, and X. You, "Integral sliding mode control for starting speed sensorless controlled induction motor in the rotating condition," *IEEE Trans. Power Electron.*, vol. 35, no. 4, pp. 4105–4116, Apr. 2020.

[31] K. A. Abuhasel, F. F. M. El-Sousy, M. F. El-Naggar, and A. Abu-Siada, "Adaptive RCMAC neural network dynamic surface control for permanent-magnet synchronous motors driven two-axis XY table," *IEEE Access*, vol. 7, pp. 38068–38084, 2019.

[32] R. Sadeghi, S. M. Madani, M. Ataei, M. R. A. Kashkooli, and S. Ademi, "Super-twisting sliding mode direct power control of a brushless doubly fed induction generator," *IEEE Trans. Ind. Electron.*, vol. 65, no. 11, pp. 9147–9156, Nov. 2018.

[33] A. Chalanga, S. Kamal, L. M. Fridman, B. Bandyopadhyay, and J. A. Moreno, "Implementation of super-twisting control: Super-twisting and higher order sliding-mode observer-based approaches," *IEEE Trans. Ind. Electron.*, vol. 63, no. 6, pp. 3677–3685, Jun. 2016.

[34] Z. Feng and J. Fei, "Super-twisting sliding mode control for micro gyroscope based on RBF neural network," *IEEE Access*, vol. 6, pp. 64993–65001, 2018.

[35] C. Lascu, A. Argeseanu, and F. Blaabjerg, "Supertwisting sliding-mode direct torque and flux control of induction machine drives," *IEEE Trans. Power Electron.*, vol. 35, no. 5, pp. 5057–5065, May 2020.

[36] Y. Wu, F. Ma, X. Liu, Y. Hua, X. Liu, and G. Li, "Super twisting disturbance observer-based fixed-time sliding mode backstepping control for air-breathing hypersonic vehicle," *IEEE Access*, vol. 8, pp. 17567–17583, 2020.

[37] O. A. Morfin, F. A. Valenzuela, R. R. Betancour, C. E. Castañeda, R. Ruíz-Cruz, and A. Valderrabano-Gonzalez, "Real-time SOSM super-twisting combined with block control for regulating induction motor velocity," *IEEE Access*, vol. 6, pp. 25898–25907, 2018.

[38] A. V. R. Teja, C. Chakraborty, and B. C. Pal, "Disturbance rejection analysis and FPGA-based implementation of a second-order sliding mode controller fed induction motor drive," *IEEE Trans. Energy Convers.*, vol. 33, no. 3, pp. 1453–1462, Sep. 2018.

[39] S. Krim, S. Gdaim, A. Mtibaa, and M. F. Mimouni, "FPGA-based real-time implementation of a direct torque control with second-order sliding mode control and input–output feedback linearisation for an induction motor drive," *IET Electr. Power Appl.*, vol. 14, no. 3, pp. 480–491, Mar. 2020.

[40] Y. B. Shtessel, J. A. Moreno, F. Plestan, L. M. Fridman, and A. S. Poznyak, "Super-twisting adaptive sliding mode control: A Lyapunov design," in *Proc. 49th IEEE Conf. Decis. Control (CDC)*, Atlanta, GA, USA, Dec. 2010, pp. 5109–5113.

[41] Y. Shtessel, M. Taleb, and F. Plestan, "A novel adaptive-gain supertwisting sliding mode controller: Methodology and application," *Automatica*, vol. 48, no. 5, pp. 759–769, May 2012.

[42] A. Levant, "Principles of 2-sliding mode design," *Automatica*, vol. 43, no. 4, pp. 576–586, Apr. 2007.

[43] D. Liang, J. Li, and R. Qu, "Sensorless control of permanent magnet synchronous machine based on second-order sliding-mode observer with online resistance estimation," *IEEE Trans. Ind. Appl.*, vol. 53, no. 4, pp. 3672–3682, Jul./Aug. 2017.

[44] T. Gonzalez, J. A. Moreno, and L. Fridman, "Variable gain super-twisting sliding mode control," *IEEE Trans. Autom. Control*, vol. 57, no. 8, pp. 2100–2105, Aug. 2012.

[45] C. Gong, W.-K. Sou, and C.-S. Lam, "Second-order sliding-mode current controller for LC-coupling hybrid active power filter," *IEEE Trans. Ind. Electron.*, vol. 68, no. 3, pp. 1883–1894, Mar. 2021.

[46] H. M. M. Adil, S. Ahmed, and I. Ahmad, "Control of MagLev system using supertwisting and integral backstepping sliding mode algorithm," *IEEE Access*, vol. 8, pp. 51352–51362, 2020.

[47] P. Gao, G. Zhang, H. Ouyang, and L. Mei, "An adaptive super twisting nonlinear fractional order PID sliding mode control of permanent magnet synchronous motor speed regulation system based on extended state observer," *IEEE Access*, vol. 8, pp. 53498–53510, 2020.

[48] Z. Li, S. Zhou, Y. Xiao, and L. Wang, "Sensorless vector control of permanent magnet synchronous linear motor based on self-adaptive super-twisting sliding mode controller," *IEEE Access*, vol. 7, pp. 44998–45011, 2019.

[49] D. Liang, J. Li, R. Qu, and W. Kong, "Adaptive second-order sliding-mode observer for PMSM sensorless control considering VSI nonlinearity," *IEEE Trans. Power Electron.*, vol. 33, no. 10, pp. 8994–9004, Oct. 2018.

[50] S. R and B. Singh, "Sensorless predictive control of SPMSM-driven light EV drive using modified speed adaptive super twisting sliding mode observer with MAF-PLL," *IEEE J. Emerg. Sel. Topics Ind. Electron.*, vol. 2, no. 1, pp. 42–52, Jan. 2021.

[51] H. Wang, X. Ge, and Y.-C. Liu, "Second-order sliding-mode MRAS observer-based sensorless vector control of linear induction motor drives for medium-low speed maglev applications," *IEEE Trans. Ind. Electron.*, vol. 65, no. 12, pp. 9938–9952, Dec. 2018.

[52] K. G. Vamvoudakis and F. L. Lewis, "Online actor–critic algorithm to solve the continuous-time infinite horizon optimal control problem," *Automatica*, vol. 46, no. 5, pp. 878–888, May 2010.

[53] R. Bellman and S. Dreyfus, *Applied Dynamic Programming*. Princeton, NJ, USA: Princeton Univ. Press, 1962.

[54] P. J. Werbos, "Neural networks for control and system identification," in *Proc. 28th IEEE Conf. Decis. Control*, Tampa, FL, USA, vol. 1, Dec. 1989, pp. 260–265.

[55] P. J. Werbos, "Approximate dynamic programming for real-time control and neural modeling," in *Handbook of Intelligent Control: Neural, Fuzzy, and Adaptive Approaches*, D. A. White and D. A. Sofge, Eds. New York, NY, USA: Van Nostrand Reinhold, 1992, ch. 13.

[56] D. Liu, Q. Wei, D. Wang, X. Yang, H. Li, *Adaptive Dynamic Programming With Applications in Optimal Control*. New York, NY, USA: Springer, 2017.

[57] F. L. Lewis, D. Vrabie, and V. L. Syrmos, *Optimal Control*. Hoboken, NJ, USA: Wiley, 2013.

[58] H. Modares and F. L. Lewis, "Optimal tracking control of nonlinear partially-unknown constrained-input systems using integral reinforcement learning," *Automatica*, vol. 50, no. 7, pp. 1780–1792, Jul. 2014.

[59] R. Kamalapurkar, H. Dinh, S. Bhasin, and W. E. Dixon, "Approximate optimal trajectory tracking for continuous-time nonlinear systems," *Automatica*, vol. 51, pp. 40–48, Jan. 2015.

[60] B. Kiumarsi and F. L. Lewis, "Actor–critic-based optimal tracking for partially unknown nonlinear discrete-time systems," *IEEE Trans. Neural Netw. Learn. Syst.*, vol. 26, no. 1, pp. 140–151, Jan. 2015.

[61] C. Mu, Z. Ni, C. Sun, and H. He, "Data-driven tracking control with adaptive dynamic programming for a class of continuous-time nonlinear systems," *IEEE Trans. Cybern.*, vol. 47, no. 6, pp. 1460–1470, Jun. 2017.

[62] R. Kamalapurkar, L. Andrews, P. Walters, and W. E. Dixon, "Model-based reinforcement learning for infinite-horizon approximate optimal tracking," *IEEE Trans. Neural Netw. Learn. Syst.*, vol. 28, no. 3, pp. 753–758, Mar. 2017.

[63] C. Lian, X. Xu, H. Chen, and H. He, "Near-optimal tracking control of mobile robots via receding-horizon dual heuristic programming," *IEEE Trans. Cybern.*, vol. 46, no. 11, pp. 2484–2496, Nov. 2016.

[64] F.-Y. Wang, H. Zhang, and D. Liu, "Adaptive dynamic programming: An introduction," *IEEE Comput. Intell. Mag.*, vol. 4, no. 2, pp. 39–47, May 2009.

[65] D. Wang, D. Liu, H. Li, and H. Ma, "Neural-network-based robust optimal control design for a class of uncertain nonlinear systems via adaptive dynamic programming," *Inf. Sci.*, vol. 282, pp. 167–179, Oct. 2014.

[66] D. Liu, D. Wang, F.-Y. Wang, H. Li, and X. Yang, "Neural-network-based online HJB solution for optimal robust guaranteed cost control of continuous-time uncertain nonlinear systems," *IEEE Trans. Cybern.*, vol. 44, no. 12, pp. 2834–2847, Dec. 2014.

[67] Y.-J. Liu, L. Tang, S. Tong, C. L. P. Chen, and D.-J. Li, "Reinforcement learning design-based adaptive tracking control with less learning parameters for nonlinear discrete-time MIMO systems," *IEEE Trans. Neural Netw. Learn. Syst.*, vol. 26, no. 1, pp. 165–176, Jan. 2015.

[68] Z. Cao, Q. Xiao, R. Huang, and M. Zhou, "Robust neuro-optimal control of underactuated snake robots with experience replay," *IEEE Trans. Neural Netw. Learn. Syst.*, vol. 29, no. 1, pp. 208–217, Jan. 2018.

[69] F. F. M. El-Sousy and K. A. Abuhasel, "Nonlinear robust optimal control via adaptive dynamic programming of permanent-magnet linear synchronous motor drive for uncertain two-axis motion control system," in *Proc. IEEE Ind. Appl. Soc. Annu. Meeting (IAS)*, Sep. 2018, pp. 1–12.

[70] J. Na, G. Li, B. Wang, G. Herrmann, and S. Zhan, "Robust optimal control of wave energy converters based on adaptive dynamic programming," *IEEE Trans. Sustain. Energy*, vol. 10, no. 2, pp. 961–970, Apr. 2019.

[71] F. F. M. El-Sousy and K. A. Abuhasel, "Nonlinear robust optimal control via adaptive dynamic programming of permanent-magnet linear synchronous motor drive for uncertain two-axis motion control system," *IEEE Trans. Ind. Appl.*, vol. 56, no. 2, pp. 1940–1952, Mar. 2020.

[72] B. Igelnik and Y.-H. Pao, "Stochastic choice of basis functions in adaptive function approximation and the functional-link net," *IEEE Trans. Neural Netw.*, vol. 6, no. 6, pp. 1320–1329, Nov. 1995.
[73] F. Liu, J. Sun, J. Si, W. Guo, and S. Mei, "A boundedness result for the direct heuristic dynamic programming," *Neural Netw.*, vol. 32, pp. 229–235, Aug. 2012.
[74] Y. Sokolov, R. Kozma, L. D. Werbos, and P. J. Werbos, "Complete stability analysis of a heuristic approximate dynamic programming control design," *Automatica*, vol. 59, pp. 9–18, Sep. 2015.
[75] J. Si and Y.-T. Wang, "Online learning control by association and reinforcement," *IEEE Trans. Neural Netw.*, vol. 12, no. 2, pp. 264–276, Mar. 2001.
[76] D. G. Luenberger, *Introduction to Dynamic Systems*. New York, NY, USA: Wiley, 1979.

FAYEZ F. M. EL-SOUSY (Member, IEEE) received the B.Sc. degree in electrical engineering from Menoufia University, Egypt, in 1988, and the M.Sc. and Ph.D. degrees in electrical engineering from Cairo University, Giza, Egypt, in 1994 and 2000, respectively.

From 1988 to 2019, he was with the Department of Power Electronics and Energy Conversion, Electronics Research Institute, Giza, where he was a Full Professor. From August 1995 to June 2000, he was a Lecturer with the Department of Electrical Engineering, October Six University, Giza. From August 2000 to June 2003, he was an Assistant Professor with the Department of Electrical Engineering, October Six University. From April 2004 to February 2007, he was a Postdoctoral Visiting Researcher with the Graduate School of Information Science and Electrical Engineering, Kyushu University, Fukuoka, Japan. From 2007 to 2010, he was an Associate Professor and the Chair of the Electrical Engineering Department, College of Engineering, King Saud University, Riyadh, Saudi Arabia. From 2010 to 2014, he was the Chair of the Electrical Engineering Department, College of Engineering, Salman bin Abdulaziz University, Al-Kharj, Saudi Arabia. Since 2014, he has been a Full Professor with the Electrical Engineering Department, College of Engineering, Prince Sattam bin Abdulaziz University, Saudi Arabia. His research interests include modeling and control of motor drives, motion-control systems, wind energy systems, digital signal processing-based computer control systems, computational intelligent of power electronics, electric drives and power systems, intelligent control theories including fuzzy logic, neural networks, and wavelets, nonlinear control, optimal control, and robust control. He is currently interested in the intelligent control of smart grid and DC micro grid.

FARHAN A. F. ALENIZI (Member, IEEE) received the B.Sc. and M.Sc. degrees in electrical engineering from King Saud University, in 1999 and 2006, respectively, and the Ph.D. degree in electrical engineering and computer science from the University of California, Irvine, in 2017. He has been a Faculty Member with the Department of Electrical Engineering, PSAU University, Saudi Arabia, since 2010. He is currently working as an Assistant Professor with PSAU University. Besides his academic experience, he worked for ten years at the Saudi Telecom Company (STC), a leading telecommunication company in the Middle East as a Designer and a Consultant in the satellite and optical fiber transmission networks. His research interests include images and video processing, signal processing, discrete signal processing (DSP), images and video watermarking, 3D mesh objects watermarking, and secure multimedia exchanges.